UCRL-16962

Cy.2

University of California

Ernest O. Lawrence Radiation Laboratory

HEAVY CHARGED-PARTICLE BEAMS

Mudundi R. Raju, John T. Lyman,
Tor Brustad, and Cornelius A. Tobias

Berkeley, California

DISCLAIMER

Chapter in book "Radiation Dosimetry,"
Vol. III, Second edition,
Academic Press

UCRL-16962

UNIVERSITY OF CALIFORNIA

Lawrence Radiation Laboratory
Berkeley, California

AEC Contract No. W-7405-eng-48

HEAVY CHARGED-PARTICLE BEAMS

Mudundi R. Raju, John T. Lyman,
Tor Brustad, and Cornelius A. Tobias

June 30, 1967

HEAVY CHARGED-PARTICLE BEAMS

Mudundi R. Raju, John T. Lyman,
Tor Brustad, and Cornelius A. Tobias

June 30, 1967

HEAVY CHARGED-PARTICLE BEAMS[1]

Mudundi R. Raju,* John T. Lyman,
Tor Brustad,† and Cornelius A. Tobias

Donner Laboratory and Lawrence Radiation Laboratory
University of California
Berkeley, California

June 30, 1967

ABSTRACT

The nature of the principal interactions of heavy charged particles with matter is discussed with particular emphasis on energy loss, range-energy relations, and multiple scattering. Following this, there is a discussion of the instruments which have been especially useful for measurements of charged particle beams (e.g., ionization chambers, Faraday cups, secondary emission monitors, activation dosimeters, and semiconductor detectors). The next section describes the measurements of heavy-charged-particle beams (e.g., Bragg curves, number-distance curves) useful for radiobiologic and radiotherapeutic applications. The final section is a description of some of the procedures of exposure which have been used for various biologic and medical problems.

I. INTRODUCTION

Accelerated heavy charged particles are of interest in radiation biology and nuclear medicine because of their physical properties. Since the mass of heavy charged particles is many times that of electrons, the angle of scattering in a given collision is reduced approximately by the ratio of the masses. Hence, heavy charged particles produce a more sharply defined beam than electrons of comparable velocity, and thus undesirable side scattering can be reduced to a minimum. The radiation field of heavy charged particles can also be shaped with greater precision than it can be for x-rays and gamma rays. The heavy-charged-particle beam has a definite range of penetration depending on its energy. It proceeds through a medium in very nearly a straight line, and the dose delivered by it increases as the particles slow down, giving rise to a sharp maximum known as the Bragg peak near the end of the range. These properties make possible intense irradiation of a strictly localized region within the body, with little skin dose (Tobias et al., 1952). Various types of particle accelerators that have been used to accelerate different particles to different energies have been thoroughly discussed in a review article by McMillan (1959). Hubbard (1961) has discussed accelerators for heavy ions. A comprehensive list of accelerator facilities around the world is given by Gordon and Behman (1963).

In radiation biology a key question concerns the manner in which ionizing radiation exerts its biological effects. It is well known that the magnitude of these effects depends not only on the dose, but

also on the detailed distribution of ionizing events in the tracks. Linear energy transfer (LET) is a measure of this distribution, at least to a first approximation, and the need for determining biological effects as a function of LET has long been realized. The most widely used radiations--x rays and neutrons--cause a broad distribution of LET in tissue in most cases and are therefore not very suitable for precise LET-effect studies. Heavy ions can be produced in accelerators (Brustad et al., 1960; Hubbard et al., 1961) in almost exactly monoenergetic and parallel beams, which thus are suitable for quantitative studies of biological effects by the "track-segment" method (Zirkle and Tobias, 1953; Sayeg et al., 1959; Barendsen et al., 1963). The currently available beams of heavy charged particles range from protons to argon nuclei-(with LET of less than 1 keV/μ to 2000 keV/μ), and with the acceleration of still heavier ions, the LET could be extended even higher.

Studies with various types of unicellular organisms and with mammalian cells have already indicated that biological effects probably can be divided into three classes: those that result from a single ionizing event, those due to cooperative action of two or more events, and those that could be attributed to the "thermal-spike mechanism" at very high LET. The first kind of effect is the one most commonly occurring in x ray studies. This effect depends upon pH and oxygen concentration, and can be moderated by chemical substances present during irradiation. It is partially reversible in that post-irradiation recovery can occur under certain circumstances. For example, in bacterial spores, heat

or presence of H_2S partially reverses this type of lesion (Powers et al., 1967).

A second mechanism can be said to bring about the often observed increase in RBE (relative biological effectiveness) when high-LET radiation is used. There is no general agreement as to the details of this mechanism; however Lea (1955), Howard-Flanders (1958), and others attribute it to ion clusters in the particle tracks. More recently, Tobias and Todd (1963) and Powers et al. (1967) found that damage due to this mechanism can not be reversed, as can single-event damage. The increase in chromosome breaks found at high LET is explained by somewhat similar reasoning by Neary et al. (1963). Further, it appears that the probability of damage, as measured by a "cross section," increases proportionally to the square of the LET, finally becoming saturated at very high LET. Except in rare instances, this effect is only slightly influenced by environmental modifiers (Manney et al., 1963; Lyman, 1965).

The third effect--the thermal-spike effect (Norman, 1965)--has not been very widely studied so far, no doubt because of the relatively difficult accessibility of the very-high-LET radiations. Probably the most dramatic demonstration of such effects is the production of holes a few angstroms in diameter in thin sheets of matter by individual fission recoils (Fleischer et al., 1965; Walker, 1965).

The heavy ions have also been very useful in molecular studies, probably because they can transfer a relatively large amount of energy to a single macromolecule (Pollard, 1953; Brustad and Fluke, 1958; Dolphin and Hutchinson, 1960; Brustad, 1961; Tobias and Manney,

1964; and Henriksen, 1966.) The fate of the excitation energy following such interaction is of fundamental interest, and studies of post-irradiation excited states are giving new information on the nature of interactions and energy transport in macromolecules.

Potentially, perhaps the widest interest in heavy ions is due to their applicability to studies of normal and pathologic states in multicellular organisms, particularly of the central nervous system, and of development and differentiation. These interests culminate in therapeutic applications which are steadily expanding (Lawrence and Tobias, 1965; Tobias and Todd, 1967). In this sense the most direct applications of accelerated particles is their role in production of controlled lesions in locations not easily accessible by other methods, e.g., surgery. Since heavy-ion beams travel along a straight line, they can be optically aimed; their Bragg ionization properties produce deep lesions without undue damage to intervening or deeper tissues (Wilson, 1946).

For example, much valuable information on the location and manner of homeostatic control of body functions can be obtained by creating small lesions unilaterally or bilaterally in the hypothalamus of animals (Born et al., 1959). Other studies are aimed at understanding the organization and function of the cerebral cortex. Laminar lesions are particularly useful in this context (Malis et al., 1957; Janssen et al., 1962). It is important to produce minimal-size lesions with especially sharp boundaries. The small lesions enable one to differentiate between near neighboring parts and thus to avoid unnecessary injury. Small and sharply demarcated lesions reduce the amount of scar tissue formed,

a consideration very important in medical procedures (VanDyke and Janssen, 1963). The physical properties of the heavy ions suggest that monoenergetic particles of proper range in tissue be used for production of lesions, instead of degrading a higher energy beam by absorbers. It is possible that for treating lesions with the Bragg peak, particles with atomic number of 6-12 might be ideal. Protons were first used on humans at Berkeley in 1954 (Tobias et al., 1956, 1958), when the pituitary of a patient with metastatic mammary carcinoma was irradiated. Since then therapeutic investigations have broadened continuously. At the University of Uppsala the first proton treatment of Parkinson's disease was performed (Larsson et al., 1962). At the University of Uppsala (Leksell et al., 1960; Larsson et al., 1958; Larsson, 1961), and at Harvard (Kjellberg et al., 1962 and 1964) and at Berkeley (Lawrence and Tobias, 1965) a number of other procedures are also used. Pituitary irradiation appears to be worthwhile in cases of mammary cancer, diabetes mellitus with vascular disease, malignant exophthalmus, acromegaly, and Cushing's disease. Certain types of brain tumors are also treated. Limited approaches to direct irradiation of tumor metastases have already been made, and the utilization of heavy-ion beams for direct cancer therapy promises to eliminate complications due to the oxygen effect (Tobias and Todd, 1967). The oxygen effect apparently is important in x-ray therapy, since anoxic tumor cells are more resistant to x rays than are oxygenated normal cells (Gray, 1961). Both kinds of cells are equally sensitive to high LET radiation.

Even before the advent of space flight, it became clear that protons, helium ions, and heavy ions are part of the normal radiation environment in cosmic rays and in the vicinity of the sun. Solar flares in fact constitute a major health hazard for astronauts (Van Allen, 1961; Webber, 1963, 1966), for planetary life, and for future colonizers of interplanetary space. We know now that flares consist of low- and high-energy protons, and that about 10% of the particles in large flares are helium ions. Solar flares simulated by using high-energy accelerators can be used for these studies. Moreover, heavier ions have also been detected in solar flares. In the study of the effects of these radiations on man, the mammalian radiobiology of heavy ions has become of interest. Because of the nature of the spectrum of solar-flare radiation, relatively more low-energy ions strike the superficial tissues and skin than penetrate them (see Nefedor, 1965). The difference between high- and low-LET radiations is not only in the RBE of the initial radiobiological injury in time but also it is apparent during the time the cells partially recover. Recovery from radiation effects in mammals occurs following low LET radiation, but it appears to be considerably diminished after high LET radiation.

Another interesting consideration here is that the radiation effect might be synergistic with other environmental stresses of space flight. It is necessary to know the interaction of radiation effects with those due to acceleration, temperature, and to special atmospheres in the closed environment in space vehicles. Psychological stress and its interaction with radiation effects must also be evaluated. It is expected that in a few years supersonic transport planes will carry a significant

fraction of the population at altitudes of 70,000 feet or more. At these altitudes the primary biological interest is particularly the heavy cosmic rays and the recoils produced by cosmic-ray primaries and secondaries, particularly mesons. It is known that the dose levels during flight will be quite low, but the potential biological effects of the heavy primaries have not yet been fully evaluated. Heavy primaries might constitute a particular hazard to human embryonic tissue, since radiation by heavy ions during embryogenesis could cause developmental malformations in later life. A study of micro-irradiation of cells (Zirkle and Bloom, 1953; Zirkle, 1957) and of embryos (Slater et al., 1964) has already begun in the laboratory and is one of the promising aspects of research with accelerated particles.

Negative pi mesons produce nuclear stars at the end of their tracks, and because these stars have high LET, it has been proposed that mesons might profitably be used in cancer therapy (Fowler and Perkins, 1961; Richman et al., 1966; Raju et al., 1967). Cyclotrons and linear-ion accelerators are particularly suitable for production of mesons. A meson factory producing enough intensity of negative pi mesons is being built at the Los Alamos Scientific Laboratory.

At the time of this writing, the principles of accelerating ions of any of the elements of the periodic table to biologically useful energies have been demonstrated. Should heavy-ion accelerators become prevalent, biological applications will become widespread.

The use of small cyclotrons in hospitals for producing short-lived isotopes and possibly for fast neutron therapy is now feasible due to commercial production of cyclotrons. Thus biological applications of heavy charged-particle beams is no longer restricted to a few laboratories.

II. INTERACTION OF HEAVY CHARGED PARTICLES WITH MATTER

The radiation dose received by an irradiated sample is a consequence of interactions of the charged particles with the sample material. A brief review of these interactions is given here before specific dosimetry problems are considered. For a more detailed discussion of these interactions, the reader is referred to Bichsel (this work, Vol. I, Chapter 4), Fano (1963), and Bethe and Ashkin (1953).

The interactions of heavy charged particles with matter can be broadly treated as an interaction with whole atoms, or with atomic electrons, or with nuclei. The first two interactions are due to electric charge (electromagnetic interactions) while in the latter, nuclear forces act as well as the Coulomb force.

The probability of a particle undergoing a certain type of electromagnetic interaction depends on the "nuclear impact parameter," i.e., the distance between the charged-particle trajectory and the nucleus in the absence of an interaction (Rossi, 1952).

1. When the nuclear impact parameter is much larger than the atomic dimensions, the charged particle interacts with the atom as a whole, displacing it from its normal position.

2. When the nuclear impact parameter is comparable to the atomic dimensions, the interaction is mainly between the charged particle and the atomic electrons. If the energy acquired by the electron is large compared to its binding energy, this process can be treated as an interaction between the charged particle and a free

electron. If the resulting secondary electrons are energetic enough, they can cause further ionization of atoms, and are called δ rays.

3. When the nuclear impact parameter becomes smaller than the atomic radius, in addition to interacting with electrons, the incoming charged particle is deflected due to the Coulomb field of the nucleus. For nuclear impact parameters smaller than nuclear radii, nuclear reactions will take place.

Thus, as a result of electromagnetic interactions, the heavy charged particles lose energy by ionization and excitation of the atoms in the medium. Successive small deflections due to Coulomb interaction between the charged particle and the nucleus of the medium (multiple scattering) cause the particle beam to spread transversely as it passes through the medium. Elastic collisions with atoms play an insignificant role in the energy loss of heavy charged particles, except at very low energies. The energy at which elastic collisions with atoms become more important than the electronic collisions in the energy-loss process varies with the heavy charged particle under consideration (Lindhard, 1964; Snyder and Neufeld, 1957); for example, this energy is 1.5 keV for protons, 94 keV for carbon ions, and 180 keV for oxygen ions. It has been shown by Jung (1965) that the radiobiological effect is very significant for protons of energies less than 1 keV. This result confirms the importance of elastic collisions with atoms at such low energies.

Inelastic collisions with nuclei, i.e., those in which nuclear reactions occur, depend primarily on the type and energy of the heavy charged particle and on the nature of the nuclei in the medium.

The penetration of secondary particles produced in these reactions will have to be considered separately. (See Sondhaus and Evans, Ch. 26, this volume). Table I (Bobkov et al., 1964) shows the probabilities of nuclear interaction for protons penetrating different thicknesses of carbon and lead absorbers (see also Janni, 1966). When nuclear interactions are important, the beam intensity decreases exponentially with increasing absorber thickness.

Table I. Probability of proton nuclear interactions as a function of absorber thickness.

Proton energy (MeV)	Shielding thickness (g/cm^2)	Residual energy (MeV)		Portion of protons not undergoing nuclear interactions in the shielding	
		Carbon	Lead	Carbon	Lead
100	5	61	81	0.95	0.98
150	5	123	135	0.95	0.98
	10	92	121	0.90	0.95
300	5	285	290	0.95	0.98
	10	265	280	0.91	0.96
	50	87	200	0.61	0.80
600	5	590	590	0.95	0.97
	10	575	580	0.90	0.95
	50	480	530	0.58	0.77
	100	340	455	0.33	0.59
	150	162	385	0.19	0.46
1000	5	990	990	0.95	0.98
	10	980	980	0.90	0.95
	50	900	940	0.60	0.79
	100	800	880	0.34	0.62
	150	685	820	0.20	0.49
	200	570	760	0.12	0.38

A. ENERGY LOSS

As they pass through matter, heavy charged particles lose energy chiefly through interactions with atomic electrons. This process leads to gradual decrease of their energy as they pass through the stopping medium. For example, the residual energy of a 160-MeV proton beam as it passes through water is shown in Fig. 1. The rate of energy loss is proportional to the square of the charge of the incident heavy particle and approximately inversely proportional to its energy. As the particle proceeds through the medium, it slows down gradually, and hence its rate of energy loss increases. At low velocities, the effective charge of the particles is reduced; in addition, the rate of energy loss will decrease at very low velocities. The heavy charged particle continues to decelerate until its energy is reduced to the thermal energy of the atoms in the medium.

The deceleration process of heavy particles during the time the particle is fully charged can be adequately treated by theory. When the charged particle is slow enough to capture electrons (below 2 MeV for alpha particles and 0.4 MeV for protons), the theoretical problems become difficult, and the effect of such capture of electrons by the charged particle on its range is taken empirically from the existing experimental data. The average energy loss per g/cm^2 of the path (stopping power) in the medium for a nonrelativistic particle is given by

$$S = \frac{0.307}{\beta^2} \quad \frac{z^2}{A} \cdot B, \tag{1}$$

with B equal to $Z[\log 2mc^2\beta^2 - \log(1-\beta^2) - \beta^2 - \log I] - C$, β the velocity, z the charge number of the incident particle, A the atomic weight of the medium, B the stopping number, Z the nuclear charge of the absorber, I the average excitation potential of the medium, and C the sum of the shell corrections (Walske, 1952, 1956). For practical calculations of stopping power of protons, see Chap. 4, Section II. C or II. H. The stopping power of water and lead for protons over a wide range of energies is shown in Fig. 2.

The stopping power formula, Eq. (1), can be used for low-energy ions if the effective charge z^* is used for z. For C^{12} and A^{40} heavy ions, for example, the maximum specific ionization occurs at energies of approximately 8 and 65 MeV, respectively (Northcliffe, 1964). At lower energies the decrease of the net charge of the ion overcompensates the effect of increase in energy loss at lower velocities. This effect is the same, on an exaggerated scale, as that for protons at much lower energies.

Tables of stopping power of various elements for various heavy charged particles are given in Chap. 4 and by Barkas and Berger, (1964); Trower, (1966); Williamson et al. (1966), Janni (1966), and Bichsel (1963).

It follows from Eq. (1) that the ratio of the stopping power for a particle with charge number z_1 to that of another particle with charge number z_2 is given by:

$$\frac{S_1}{S_2} = \frac{z_1^2}{z_2^2}, \qquad (2)$$

when the particles travel with equal velocity through the same material. Hence, knowing the energy loss of protons, one can calculate the energy loss of any other heavy charged particle from Eq. (2).

The stopping powers of two substances for a particle with a given velocity may be compared independently of their densities by considering the relative mass stopping power Sm:

$$Sm = \frac{Z_1 A_2}{Z_2 A_1} \cdot \frac{B_1}{B_2}, \tag{3}$$

where A is the atomic weight of the substance.

In obtaining the stopping power of a compound we assume that the contribution from the individual atoms that comprise the compound are additive (Bragg's rule). This method neglects any effects of the electronic binding in the molecular compound. Deviations from the additivity rule exist (see Chap. 4), but these are generally not significant in radiobiology except at low energies. Thus we can calculate the stopping power of compounds from the stopping-power data of the various elements such as those tabulated by Barkas and Berger (1964). It is important to note that the stopping-power values derived in this way apply to compounds which at a macroscopic level are homogeneous and isotropic. This raises a conceptual problem in their evaluation in radiobiology at the submicroscopic level, since living cells are anisotropic and inhomogeneous in their chemical composition. Usually, one also ignores variations in the density of subcellular particles. Engstrom and Lindstrom (1958) have shown, however, by the method of quantitative x-ray microscopy, that in certain cells the density of the nucleus

may be twice that of the cytoplasm. The density of DNA preparations separated from living cells by homogenizing the cells and centrifuging the density gradient, is between 1.5 and 1.6.

B. RANGE-ENERGY RELATION

A monoenergetic beam of heavy charged particles traversing matter will lose energy by very many collisions with the electrons of the medium while the total number of particles in the beam remains essentially the same (see Table I, though). The particles will finally be stopped in the medium after they have penetrated approximately equal thicknesses of the absorber. The mean distance traveled in the medium by particles of a given energy is called their range and is usually expressed in g/cm^2. The absorption of electromagnetic radiation, in contrast, is exponential. The ionization energy loss is subjected to statistical fluctuations and hence there will be fluctuations in the ranges of individual particles. The fluctuation in ranges are known as straggling, and amount to about 1% of the total range (Wilson, 1946). The energy-loss fluctuations are discussed in detail in Section IV.

Figure 3 shows an integral-range curve, the plot of the number of particles in the beam penetrating to a certain depth. The thickness R_p of the medium traversed by half the particles is called the median projected range, and the thickness R_e of the medium obtained by the intersection of the tangent at the point of steepest descent with the X-axis representing the thickness of the medium, is called the extrapolated range. The difference between the median range and the extrapolated range is related to the straggling parameter (Hubbard and MacKenzie, 1952). For a given range, straggling is less as we go to heavier ions. For a given particle, straggling increases with the energy of the particle. At higher energies the number-distance

curve shows the exponential decrease due to nuclear collisions (see Fig. 21).

From Eq. (1) the distance ΔR traveled through an absorber by a particle of mass M and atomic number z for a decrease in energy from E_1 to E_2 is

$$\Delta R_{z,\,M}(E_1 - E_2) = \int_{E_2}^{E_1} (1/S)\, dE. \tag{4}$$

In principle, the range of a particle of initial energy E_0 is obtained by integrating from E_0 to zero energy (see Chap. 4).

Since the value of the integral in Eq. (4) is dependent only on the velocity of the particle, the ranges of two different particles passing through the same stopping material with equal initial velocities are related by

$$R_1(v) = \frac{M_1}{M_2}\,\frac{z_2^2}{z_1^2}\, R_2(v) - C_R(z_1, z_2). \tag{5}$$

The constant is independent of velocity; its value is small but not zero and is determined empirically for particles of different charge. It takes into account the capture and loss of electrons at low velocities. For range differences above this region the constant C_R subtracts out, and a single range-energy relation is sufficient for different particles in each stopping material. Theoretical range-energy and stopping-power relationships among various heavy ions in water are given in Fig. 4 (Steward and Wallace, 1966). Several theoretical range-energy tables are available (see Chap. 4, and Barkas and Berger, 1964;

Williamson et al., 1966; and Janni, 1966). A computer program for the calculation of the energy loss of heavy charged particles is given by Bichsel (1967).

C. MULTIPLE SCATTERING OF HEAVY CHARGED-PARTICLE BEAMS

When a parallel beam of particles passes through a medium, the particles in the beam spread transversely, mainly due to Coulomb interaction between the charge of the incident particles and the nuclei of the medium. This scattering is partly the result of the cumulative effect of a number of small deflections produced by different atomic nuclei in the traversed matter, and partly due to rare large deflections. The first type of scattering is called "multiple" or "plural" depending on whether the number of contributing collisions is large or small. The second type is referred to as single scattering. For most practical applications multiple scattering through small angles, represented approximately by a Gaussian distribution, predominates over plural and single scattering. The earliest and simplest theory on multiple scattering is by Williams (1939, 1940). He assumed that the deflection of a particle due to multiple scattering is the sum of many single deflections whose probabilities are determined by the Rutherford cross-section formula. The angular distribution of particles after passing through the medium will be approximately Gaussian. The problem of multiple scattering was studied more rigorously by Moliere (1948), Bichsel and Uehling (1960), Scott (1963), and others. In practice, a simplified treatment is usually quite adequate. The simplified expression for the mean square angle of multiple scattering when the absorber thickness is small is given by

$$\langle \Theta^2 \rangle = \frac{8\pi N x Z^2 z^2 e^4}{v^2 p^2} \ln \frac{b_{max}}{b_{min}} , \qquad (6)$$

where N is the number of nuclei per cubic centimeter, x the thickness of the absorber, Ze is the charge of the medium, ze is the charge of the beam particle, p is the momentum, v is the velocity of the particle, and b_{max} and b_{min} are the maximum and minimum impact parameters. Hence the rms scattering angle is proportional to the charge of the incident particle and the medium atomic number, and (in the non-relativistic case) inversely proportional to the energy of the particle.

The standard deviation of the Gaussian distribution, which represents the effect of multiple scattering at a distance X_0 from the absorber edge for a particle beam having an initial range R_0 and residual range R, is given by

$$\sigma^2 = \int_R^{R_0} \bar{\alpha}^2 (R' - R + X_0)^2 \, dR' , \qquad (7)$$

where $$\bar{\alpha}^2 = \lim_{x \to 0} \langle \Theta^2 \rangle / x.$$

If one is interested in finding the width of the Gaussian distribution inside the absorber, then X_0 in the above expression is zero. It can be seen that the width of the Gaussian distribution representing the multiple scattering increases with the increase in X_0, even if the thickness of the scattering medium remains the same.

Starting from Williams' theory of multiple scattering and making some reasonable assumptions, Preston and Koehler (1967) obtained the following empirical expressions for the standard deviation

σ_0 in centimeters at the end of the range R_0 for a proton beam of originally negligible diameter:

$$\sigma_0 = 0.0307\ R_0 \text{ (protons in water)}, \tag{8}$$

$$\sigma_0 = 0.045\ R_0 \text{ (protons in aluminum)}. \tag{9}$$

Figure 5 gives the standard deviation σ at any fraction of the proton range in terms of the standard deviation σ_0 at the end of the range. It can be seen from Fig. 5 that the Gaussian width due to multiple scattering increases rapidly near the end of the range. If the incident beam profile is close to a Gaussian distribution of width σ_i in the absence of the scattering material, then the standard deviation due to scattering in the medium can be obtained from the measured standard deviation σ_m by using the expression

$$\sigma^2 = \sigma_m^2 - \sigma_i^2. \tag{10}$$

The effect of multiple scattering for an incident beam described by a function $f(x, y, z)$ is given by

$$I(x,y,z) = \frac{1}{\pi\sigma_x^2} \int_{y'} \int_{z'} \exp\left\{-\left[\frac{(z-z')^2 + (y-y')^2}{2\sigma_x^2}\right]\right\} f(x, y', z')dy'dz'. \tag{11}$$

Figure 6 gives computed values of $I(x, y, z)$ for 910-MeV helium-ion beam passing through a water medium at different fractions of the residual range (Sperinde, 1967). It can be seen from Fig. 6(a) that for a small collimated beam (2-mm diameter), the intensity at the central axis of the beam becomes smaller as the beam passes through

the medium. Hence the full width at half maximum of the beam is increased considerably near the end of the range. On the other hand, for large collimated beams (such as 20-mm diameter) it can be seen from Fig. 6(b) that the full width at half maximum, as well as the intensity on the central axis, remains essentially the same although the edges of the beams are rounded off a little. This modification of beam characteristics must be taken into consideration when narrow beams are used for radiological cutting in some biological applications.

A useful relation for proton and helium-ion beams of the same range is that the multiple scattering of a helium-ion beam is half that of a proton beam. Multiple-scattering calculations for protons are given by Janni (1966).

Preston and Koehler (1967) also calculated the intensity of the beam along the axis as a function of depth in the medium for both circular and rectangular apertures. The intensity I(x, 0, 0) on the axis at a depth x for a uniform circular beam of radius r_c is given roughly by the expression

$$I(x, 0, 0) = \frac{1}{\pi\sigma_x^2} \int_0^{r_c} 2\pi r \exp[-r^2/\sigma_x^2]\, dr = 1 - \exp[-r^2/\sigma_x^2]. \quad (12)$$

[This can be obtained from Eq. (11) as a special case.] For a uniform beam 128-MeV of protons of total range R_0 = 12 cm of water, the plots for Eq. (12) are shown in Fig. 7 for various beam sizes. It can be seen from the figure that, with a decrease in beam size, the number of particles per unit area along the axis decreases considerably as a

function of depth of penetration. The loss of particles due to nuclear interactions is neglected in the above calculations. Actually, the number of protons decreases with penetration into the medium as a result of nuclear interactions (Table I). At the same time, the average proton energy loss increases with depth as their velocities decrease, rising to a maximum near the end of the range. Hence the dose delivered by a heavy-charged-particle beam varies as a result of all these factors: scattering, nuclear absorption, and change of stopping power. The relative dose on the axis of a uniform proton beam for beams of different radii, as calculated by Preston and Koehler, are shown in Fig. 8, where it can be seen that the effect of scattering is negligible for a beam of sufficiently large radius, i.e., for $r_c >> \sigma$. For such large beams the dose deposition depends solely on absorption of particles by nuclear reactions and on change of the stopping power. On the other hand, for small collimated beams the effect of multiple scattering becomes important, and the central axis dose at depth becomes smaller due to particles scattering out.

The experimental results agree fairly well with the above-mentioned approximate calculations of multiple scattering of heavy-charged-particle beams. Some experimental data on measurements of heavy charged-particle beams will be given in Section IV.

For a given range, the Gaussian width due to multiple scattering becomes smaller as the atomic number of the heavy ions increases. Heavy ions, then, may prove to be more useful than other particles when narrow beams are needed for radiological cutting purposes (Litton et al., 1967).

III. DETECTORS OF HEAVY CHARGED PARTICLES

Many different types of detectors have been used to study heavy-charged-particle beams. We will limit our discussion to ionization chambers, Faraday cups, secondary emission monitors, and activation dosimeters, since these detectors are extensively used to measure high-energy beams. We also discuss semiconductor detectors because of their usefulness for energy and energy-loss measurements.

By limiting our discussion to these detectors, we do not imply that other detectors are not useful for measuring heavy charged-particle beams. Proportional counters, scintillation detectors, chemical dosimeters, solid-state integrating dosimeters, photographic emulsions, and calorimeters are extensively discussed in Volume II.

A. IONIZATION CHAMBERS

The instrument most often used to measure dose delivered by heavy charged particles is the parallel-plate ionization chamber. Ionization chambers have also been extensively covered by Boag in Vol. II, Chapter 9. Two types of such chambers which have been used extensively are shown in Fig. 9. The collection volume for such a chamber can be limited to the central part of the beam by making the collection electrode small. When a sufficiently large guard-ring electrode surrounds the collection electrode, the electric field is uniform and parallel. The collection volume, which must be known for the dose calculation, is then defined by the area of the collection electrode and the distance between the high-voltage and collection electrodes. The electrodes may be of thin metal foil, or of plastic material such as Mylar foil coated with an electrically conducting film.

Since nuclear-particle beams from accelerators fluctuate in intensity, the current from the ionization chamber is usually integrated in order to determine the total dose delivered. A typical arrangement for integrating small currents is shown in Fig. 10. The charge liberated in the ionization chamber is integrated by charging a capacitor C, and the potential developed across the capacitor is measured with the aid of an electrometer. It is advantageous to use an electrometer with nearly 100 percent inverse feedback so that the collection electrode is always held effectively at ground potential. This reduces (a) the collection of stray ions from regions of the chamber outside the intended sensitive volume, (b) leakage of charge from the collector to ground, and (c) the time constant.

The Bragg-Gray principle as it applies to dose measurement was treated extensively by Burlin (Vol. I, Chapter 8). For heavy charged particles, however, the primary interaction which results in ionization of the gas occurs principally in the gas rather than in the wall of the chamber and hence the atomic composition of the wall is not critical. It was also shown experimentally that the effect of aluminum foils is not significantly different from that of low-atomic-number materials like Mylar (Welch, 1967).

If the charge Q in coulombs is collected from an ionization chamber located at a position, the dose D in rads to the target at that position is

$$D = \frac{10^5 QWSm}{\rho V} . \qquad (13)$$

Here V is the collection volume of the ionization chamber in cm^3, ρ is the density in g/cm^3 of the ionization chamber gas at ambient temperature and pressure, W is the energy per ion pair in eV for the gas, and Sm is the mass stopping power of the target material relative to that of the gas. The factor 10^5 comes from the conversion of the units of measurements, that is, charge per ion pair to coulombs, and eV per g to rads.

In many applications the dose must be measured by an ionization chamber away from the target: for example, when the target is an organ deep within the body and the ionization chamber is at the surface. The dose received by the target differs from the dose

measured at the surface because of divergence of the beam, scattering by intervening material, and the Bragg ionization effect. Then the dose D_A delivered to the target at point A can be calculated from the charge Q collected from an ionization chamber located at point B near the surface of the subject, by the relation

$$D_A = \frac{10^5 Q W Sm K}{V\rho} \quad . \tag{14}$$

Here Sm is the mass stopping power of the target material relative to that of the ionization-chamber gas for particles with the energy of those at point A. Values of Sm can be calculated from tabulated stopping-power data (Barkas and Berger, 1964). The average energy of the particles at point A can be determined from the initial energy and the amount of energy loss through the absorber by means of the range-energy relations. K is the ratio of the energy loss per gram of gas in an ionization chamber at position A compared to the energy loss in the ionization chamber located at position B.

The factor K can be determined experimentally by constructing a phantom of material equivalent in absorbency to the subject, and measuring the charge collected in two ionization chambers located at B, near the surface of the phantom, and at A, the target point within the phantom. Then K is obtained from the relation

$$K = \frac{Q_A W_A V_B \rho_B}{Q_B W_B V_A \rho_A} \tag{15}$$

where the subscripts refer to the ionization chambers located at points A and B, and ρ_A and ρ_B are the densities of the gases in the ionization chambers at points A and B. The values of W for different gases are discussed by Myers (Vol. I, Chapter 7). An additional correction to the dose measurement for any non-uniform intensity distribution of the beam may be required (Birge and Sayeg, 1959).

In the design of chambers, pulse characteristics of the beams must be considered, and the collection voltage must be reasonably high to ensure full ion collection (Boag, Vol. II, Chapter 9). The question of the magnitude of losses due to columnar recombination in a single track is still not completely solved.

B. FARADAY CUP

The Faraday cup (Chamberlain et al., 1951; Palmieri and Goloskie, 1964; and Santoro and Peelle, 1964) is often used as a primary standard to determine the number of particles in a charged-particle beam. The charge-collection efficiency of a well-designed cup is independent of the beam intensity. The Faraday cup consists of an absorber block, thick enough to stop all of the primary beam and all of its secondary charged particles. This block, generally cup-shaped, is supported by insulators within an evacuated chamber. Care must be taken in designing the Faraday cup so that the net charge collected is only that of the beam. A typical Faraday cup is shown in Fig. 11. The block must be wider than the diameter of the beam so that particles are not scattered out of the sides of the block. For example, for 340-MeV protons the radius of the block should be at least 1.5" greater than the radius of the beam (Aamodt et al., 1952). The cup should be deep so that the solid angle through which electrons may escape is small. Secondary electrons should be prevented from entering or leaving the collection block. A magnetic field of approximately 1000 gauss oriented perpendicular to the axis of the beam is sufficient to cause low-energy secondary electrons to return to the surfaces from which they are emitted. Detailed calculations of secondary electron trajectories in a Faraday cup magnetic field are discussed by Pruitt (1966).

If an ion pump or an ionization gauge is used in connection of the vacuum system of the Faraday cups, spurious leakage currents may be caused; during measurements, it may be advisable to shut these instruments off.

Because the Faraday cup must be thick enough to stop the primary particles, as well as their secondaries, the size of a Faraday cup to be used for accurate measurements of protons of energies greater than say 400 MeV is somewhat impractical.

In many applications for which the entire energy of the particles is expended in the target, the target itself may form the Faraday cup. The number of particles N stopped by the Faraday cup is given by the relation

$$N = \frac{Q_F}{ze} \tag{16}$$

where Q_F is the charge in coulombs collected by the Faraday cup, z is the average number of charges carried by a particle, and e is the electronic charge in coulombs. Under these conditions, the total energy (U) transferred (in MeV) is

$$U = N E. \tag{17}$$

where E is the energy of the particle entering the cup.

Often the quantity of interest is the number of particles per unit area, also called the particle fluence Φ (ICRU, 1962).

$$\Phi = \frac{\Delta N}{\Delta a} . \tag{18}$$

To determine the fluence over a small area from the total number of particles, it is necessary to know the profile of the beam, since the

beam may not be of uniform intensity over its entire area (a). Knowing the particle fluence (particles/cm^2) in the target material, one can calculate the dose D in rads from the following equation

$$D = -1.602\ \Phi\left(\frac{1}{\rho}\frac{dE}{dx}\right)\ 10^{-8} \tag{19}$$

where $-\frac{1}{\rho}\frac{dE}{dx}$ is the mass stopping power (S) of the target material in MeV-g^{-1}-cm^2.

By comparing the charge Q_F collected on the Faraday cup with the charge Q_I collected in an ionization chamber that is sensitive over the entire area of the beam, one can obtain directly the specific ionization p (in ion pairs per cm) for the particular beam of particles used and for the particular gas in the ionization chamber. If N is the number of particles that pass through the ionization chamber with electrode spacing d in centimeters, we have

$$Q_I = N d p e. \tag{20}$$

If the same number of particles N is collected in the Faraday cup, Eqs. (16) and (20) give

$$\frac{Q_I}{Q_F} = \frac{pd}{z}\ . \tag{21}$$

The specific ionization p is related to the specific energy loss of the particle by

$$p = -\frac{1}{W}\frac{dE}{dx} , \tag{22}$$

where W is the energy required to form an ion pair in the ionization chamber gas.

Then Eq. (21) can be rewritten as

$$\frac{Q_I}{Q_F} = -\frac{d(dE/dx)}{z\,W} . \tag{23}$$

Hence, the ratio Q_I/Q_F is proportional to the ratio $\frac{dE/dx}{W}$. If the specific energy loss of the incident particles is known, the value of W for the particular beam used and for the particular gas in the ionization chamber can be determined from this ratio. But if the specific energy loss of the beam is not known, it can be determined from the measured ratio Q_I/Q_F with a given value of W.

C. SECONDARY EMISSION MONITOR

The secondary emission monitor is particularly useful in high-intensity radiation fields where ionization chambers are not suitable because of incomplete ion collection due to recombination (Tautfest and Fechter, 1955). In a secondary emission monitor the charge collected is due to electron transfer between the high voltage and the collection electrodes which are in ultra-high vacuum ($\approx 10^{-8}$ torr), unlike the ionization chamber where the charge collected results from the ionization in the gas. This has been discussed by Boag (Vol. II, Chapter 9).

A typical secondary emission monitor that is used at Berkeley cyclotrons to monitor intense beams is shown in Fig. 12. The relative number of electrons lost from the collector foils per incident particle as a function of applied voltage for a secondary emission monitor in use at Berkeley is shown in Fig. 13. The response of the secondary emission monitor can be calibrated by means of a Faraday cup or an ionization chamber. In order to obtain reproducibility with this monitor, it is very important that the surface of the foils is free from adsorbed material. The response of the secondary emission monitor is linear with particle flux (number of particles per unit time).

D. ACTIVATION DOSIMETER

Heavy charged particles produce radioactive isotopes by inelastic nuclear interactions. The induced activity of the sample may be used as an independent measure of the dose. Activation dosimetry can be used to determine either particle flux in the beam or the particle flux density over a small area. One of the most common monitor reactions is the C^{12} (p, pn) C^{11} reaction (Cumming, 1963; Measday, 1966). Activation analysis with charged particles is extensively covered by Tilbury (1966). The γ radiation from annihilation of the positron from the C^{11} is counted to determine the activity. The saturation activity A_∞ --that is, the maximum obtainable activity for a given particle flux--can be derived from the actual activity at t minutes after the end of the irradiation $A_c(t)$ by the following equation:

$$A_\infty = \frac{A_c(t)}{e^{-\lambda t}(1-e^{-\lambda T})}, \tag{24}$$

where λ is the decay constant and T is the irradiation time. The particle flux is given by

$$f = \frac{A_\infty M}{N_0 \sigma \xi}, \tag{25}$$

where M is the molecular weight of the target material of the activation dosimeter (commonly CH_2) N_0 is Avogadro's number, ξ is the thickness of the sample in g/cm^2, and σ is the cross section for the reaction.

Other useful isotopes are the positron emitters O^{15} and N^{13}. Activation dosimetry may be used to check dose actually received by a biological test object in vivo. It is quite practical, for example, to measure the activation from a few hundred rads of protons on a single Drosophila, which weighs only about 1 mg.

The induced C^{11} activity has been measured by the whole-body counter in humans who received a therapeutic dose of protons or helium ions (Sargent, 1962). Much of the C^{11} induced activity ends up in carboxyhemoglobin and some of this is exhaled as $C^{11}O$.

E. SEMICONDUCTOR DETECTOR

Semiconductor detectors, solid-state analogs of ionization chambers, are discussed by Fowler (Chapter 14, Vol. II). In semiconductors the charge carriers are electrons and holes. The use of a solid as a detector is attractive because the sensitive layer can be very thin but still allow much energy to be deposited. Another advantage results from the small amount of energy required to produce an electron-hole pair (≈ 3.75 eV in silicon) (Goulding, 1965). Nearly ten times as much charge is released for a given energy loss in silicon as in gas. This leads to smaller statistical fluctuations in the number of pairs and, hence, improved energy resolution over that of gas-filled counters. The collection time of the charge produced by the ionizing radiation in the semiconductor detectors is very short because of the high mobility of carriers in the electric field and the small distance between the electrodes. An attractive feature of these detectors is that their response is proportional to the deposited energy. These devices are very useful for measuring energy and energy loss as discussed in the next section.

IV. MEASUREMENT OF HEAVY CHARGED-PARTICLE BEAMS

A. THE BRAGG IONIZATION CURVE

A Bragg curve is a plot of the relative specific ionization of a collimated beam of particles plotted as a function of the thickness of absorber that the beam has traversed. It can be obtained experimentally by taking the ratio of current from two ionization chambers, one of which is placed after and the other before a variable absorber, as shown in Fig. 14. Within the energy range of interest here, the specific energy loss increases with decreasing particle velocity, reaching a maximum near the end of the particle range; consequently, the relative specific ionization rises with increasing absorber thickness and reaches a maximum near the mean range of the particles.* The Bragg curve is distinguished from the relative specific ionization curve of an individual particle. Energy spread of the incident beam, range straggling due to statistical fluctuations in energy loss, and multiple scattering cause the Bragg curve to have a lower and wider peak than that due to a single particle. Since the amount of straggling increases almost linearly with the thickness of absorber, the monoenergetic beams of low energy show the sharpest Bragg peaks.

In Bragg curve measurements, one should plan the geometry of the apparatus so that the secondary particles coming out of the collimators used to define the beam do not add considerably to the ionization in the second ionization chamber. In addition, the second ionization chamber that detects the transmitted beam from the variable absorber should be large enough to cover the entire area of the transmitted beam.

If the collection area of the second ionization chamber is limited to the central area of the beam, a curve of different shape from the Bragg curve is obtained. This curve is called the central-axis depth-dose curve.

The dose delivered to the medium at the beam entrance is called the plateau dose, and the dose at the Bragg peak the peak dose. The physical parameters of interest are the peak-to-plateau ratio and the width of the Bragg curve. The peak-to-plateau ratio is a very sensitive function of momentum spread (the same effect as energy spread) of the beam. With increasing momentum spread, the peak-to-plateau ratio is reduced considerably with concomitant increase in the width of the Bragg curve. With increasing energy of the particles, the range too is increased and this results in increase in range straggling. This effect also reduces the peak-to-plateau ratio and increases the width of the curve. In addition, with increasing energy of the particles more particles are removed from the beam because of nuclear interactions (see Section II. 3) before they reach the Bragg peak, and this also results in a reduction in peak-to-plateau ratio. A computer program for calculating Bragg curves for heavy ion beams is available (Litton, 1967). The central-axis depth-dose distribution of beams of protons and helium ions of different energy are shown in Fig. 15.

Shown in Fig. 16 are Bragg curves of various heavy-ion beams, all with initial energy of 10.4 MeV/amu. At zero absorber thickness, the particle velocities are the same and hence the square of the effective charge of the heavy ions is proportional to the specific ionization.

A differential ionization chamber is useful to determine the position of the Bragg peak and also to check the changes in the beam energy (Larsson, 1961; Hanna and Hodges, 1965). The collecting electrode is located between two high-voltage electrodes which are maintained at opposite polarity. If the first foil is negative with respect to the second foil, a positive signal is obtained from the collector electrode when the absorber is less than that needed to reach the peak. The exact location of the peak is determined by the amount of absorber needed to make the response of the two halves of the chamber equal but of opposite magnitude. Beyond the Bragg peak a negative signal is obtained from the ionization chamber until the absorber is thick enough to stop the beam completely. The large volume ionization chamber shown in Fig. 9 can be operated as a differential ionization chamber by applying high voltages of different polarity to the high-voltage foils.

B. BEAM PROFILES AND ISODOSE CONTOURS

For many applications of heavy charged-particle beams, one needs to know the three-dimensional dose distribution in the irradiated material, and for such measurements, it is important that the sensitive volume of the device is small relative to the cross section of the beam and has a high sensitivity. Small semiconductor devices are suitable for this application. An example of such a semiconductor device is a miniature silicon diode 0.1 cm in maximum diameter and 0.22 cm long (Koehler, 1965; Raju, 1966).

The sensitivity of these diodes is found to decrease as the dose increases due to radiation damage. This, however, need not be a limitation on their use as radiation dosimeters. If the diode is pre-exposed to high radiation doses, of the order of 10^6 rads, the sensitivity of the diode is reduced to about a third, but the sensitivity does not change significantly thereafter with further radiation exposures. The short circuit current of such a pre-exposed diode is found to be proportional to the total dose for time-averaged dose rates (proton and helium-ion beams) investigated from a few rads/min to 5000 rads/min, both at the plateau region and at the Bragg peak position.

Figure 17 shows a set of beam profiles of a 127-MeV proton beam incident on water as measured by a miniature silicon diode (Preston and Koehler, 1967). The same measurements replotted on a Gaussian scale are shown in Fig. 18. It is evident that the measured distributions are nearly Gaussian in form. These experimental results are in good agreement with the theory of multiple scattering of heavy charged-particle beams as discussed in Section II. 4.

Profiles can also be measured by using ionization chambers, particle counters, photographic films, activation analysis, thermoluminescent dosimeters, and so forth. From a series of beam profiles, a set of isodose contours can be constructed. Figure 19 shows such an isodose plot for a degraded 910-MeV helium-ion beam in water.

C. INTEGRAL-RANGE CURVES

A plot of the number of particles that passed through an absorber as a function of absorber thickness is called an integral-range curve or a number-distance curve. The number of charged particles that have passed through an absorber can be determined with particle counters such as Faraday cups. The experimental setup used to determine a integral-range curve is similar to that shown in Fig. 14, but with the second ionization chamber replaced by a particle counter. For low-energy particles, nuclear interactions can be neglected; the number of particles remains essentially constant from zero absorber to a thickness almost equal to the mean range of the particles. This is illustrated in Fig. 20. At high energies, however, particles are lost from the beam by nuclear interactions and under these conditions the integral-range curve as shown in Fig. 21 for a 910 MeV helium-ion beam has a finite slope. An estimate of the cross section for these interactions, σ_R, can be obtained from this slope. Thus

$$\sigma_R = - \frac{1}{NF} \frac{dF}{dx}, \tag{26}$$

where N is the number of atoms per cm^3 of the absorber, F is the number of particles, and $- \frac{dF}{dx}$ is the number of particles lost per centimeter (i.e., the slope of the integral-range curve).

In the energy region between a few MeV and a few BeV per amu, σ_R is approximately

$$\sigma_R \approx \pi r_0^2 (A_T^{1/3} + A_I^{1/3})^2 (1 - \frac{V_c}{E_{c.m.}}), \quad (27)$$

where r_0 is the nuclear radius, A is the atomic weight, the subscripts T and I refer to the target and incident nuclei respectively, V_c is the coulomb barrier potential, and $E_{c.m.}$ is the total kinetic energy in the center-of-mass system. Here r_0 is about 1.3×10^{-13} cm for protons and light nuclei of a few MeV per nucleon. At high energies the nuclei become partially transparent and the effective radius becomes smaller. For 910-MeV helium ions, $r_0 \approx 1.1 \times 10^{-13}$ cm (Litton et al., 1967). Additional measurements are needed to determine the exact energy dependence of r_0. The V_c, in MeV, is given by

$$V_c = 0.96 \frac{Z_T Z_I}{A_T^{1/3} + A_I^{1/3}}, \quad (28)$$

where Z is the atomic number and the subscripts are as defined before.

Calculations indicate that for proton energies from 0 to 400 MeV, the dose contribution from secondary particles heavier than protons, produced by nuclear interactions, generally does not exceed 2.5% (Turner et al., 1964, see also Blosser et al., 1964, and Wheeler, 1966). The biological effect of heavy recoils may be more important than their dose contribution would indicate, since the heavy recoils may have a very high relative biological effectiveness (Jung, 1965; Zimmer, 1966).

An estimate of the range of the particles can be obtained by considering the final section of the integral-range curve (Santoro,

1965; Santoro et al., 1966). A useful reference point is the extrapolated range which can be obtained by drawing the tangent to the integral-range curve at the point of steepest slope.

D. ENERGY-LOSS MEASUREMENTS

In most of the studies relating biological damage to the energy loss of the particles, the experimenter usually has had to rely on theoretical calculations of the energy loss. However, in many of the biological experiments, the theoretical calculations may not be adequate and can profitably be supplemented with experimental measurements. For example, in the low-energy region where electron pick-up is becoming important, one needs experimental data on effective charge (Heckman et al., 1960; Northcliffe, 1960; Schambra et al., 1960; Roll and Steigert, 1960). In the high-energy region where production of secondary particles by nuclear interactions is important, it becomes increasingly difficult to predict the relative contribution of all the secondary particles. In addition, whenever there is an uncertainty in energy spread of the primary particles, it is difficult to calculate the energy loss.

For a discussion of microscopic energy distributions, see Rossi, Chapter 2, Vol. I. Because of the advantages of semiconductor detectors, these devices are very useful for energy-loss measurements. If the detector thickness is so small that the energy deposited by the particle in it is very small compared with the energy of the particles, the detector can be used to measure energy-loss distribution. On the other hand, if the detector is thick enough to stop all the particles in the beam, then it can be used to measure energy distribution of the particles (Raju, 1965).

When an energetic charged particle passes through a detector, it loses energy by a series of collisions with the electrons of the detector material. In first approximation, the probability of an energy loss in a single electronic collision is proportional to ϵ^{-2} (Landau, 1944). Thus collisions resulting in a large energy transfer to an electron are relatively infrequent compared with small-energy-loss collisions. Even though they are relatively infrequent, the large-energy-loss collisions account for a significant proportion of the total energy transfer. This phenomenon has been theoretically investigated by Landau (1944), Symon (1952), Vavilov (1957), and others; it is often called the Landau effect. Experimental investigations have been carried out by Gooding and Eisberg (1957), Rosenzweig and Rossi (1963), and Grew (1965); all of them compared their data with the theoretical data of Symon.

In Vavilov's exact treatment, the dimensionless parameter κ is introduced.

$$\kappa = 0.150 \frac{(SZz^2)}{(A)} - \frac{(1 - \beta^2)}{(\beta^4)} , \qquad (29)$$

where S = thickness of detector in g/cm^2,

Z = atomic number of detector material,

A = atomic weight of detector material,

z = charge on incident particle,

β = velocity of incident particle ÷ velocity of light in vacuum

Here κ may be thought of as a measure of the ratio of the mean energy loss to the maximum possible energy loss in a single collision.

In cases where the parameter $\kappa >> 1$, the fluctuations are negligible and an approximately Gaussian shape of the total energy-loss distribution curve is obtained. Then the average energy loss equals the most-probable energy loss. If on the other hand $\kappa << 1$, the fluctuations are large; then the resulting energy-loss distribution curve would have a characteristic high-energy tail, thereby deviating considerably from a Gaussian distribution. In this case, the most-probable energy loss is less than the average energy loss as shown in Fig. 22. Note also that the full width at half maximum is approximately 30 percent; this is inherent in situations of fast particles passing through thin detectors. These experimental measurements of energy-loss distributions are in good agreement (Maccabee, 1966; Maccabee et al., 1966; Maccabee and Raju, 1967) with the rigorous theory of Vavilov as tabulated by Seltzer and Berger (1964). If one considers the thickness of the sensitive target of a biological sample to be equivalent to the detector thicknesses, of Eq. (29), then one can see that κ will be $< \leq 1$ for most charged particles, and therefore, there will be a broad distribution of energy-loss values within the target. If the target is small (e.g., nuclei and molecules), there may be too few collisions for the Landau theory to be valid. One must then use Poisson statistics and compensate for δ-ray escape.

E. ENERGY MEASUREMENTS

Because of these fluctuations of the energy lost in a given small thickness, there will be fluctuations in the total thickness traversed by particles in losing all their energy. This phenomenon is called range straggling and is the cumulative effect of energy-loss straggling over a large thickness of absorber (see Bichsel et al., 1957; Janni, 1966). The effect of the range straggling is to broaden the Bragg peak considerably. Since there are a large number of collisions at all energies, the range distribution is approximately Gaussian. The consequence of this effect can clearly be seen in the energy distribution of 910-MeV helium-ion beam and the 50-MeV proton beam at the Bragg peak position as shown in Fig. 23. The corresponding LET values in water are also shown in that figure. Note that the modal energy at the Bragg peak is much higher than one might expect and thus the LET is low (Raju, 1965). These measurements together with those at the Harvard cyclotron (Koehler, 1967) indicate that one can use a general rule of thumb that the most probable energy at the Bragg peak is about 10% of the initial kinetic energy.

F. DOSE MEASUREMENTS WITH SEMICONDUCTOR DETECTORS

When a negative pi meson is brought to rest in a medium, say tissue, it is captured by a constituent nucleus, which explodes into a "star" consisting of short-range and heavily ionizing fragments capable of delivering a large localized radiation dose resulting in an augmented Bragg peak. Because of the large range of energy deposition involved at the plateau and peak regions of negative pi mesons, semiconductor detectors have been used to measure depth-dose distribution. In addition, these detectors have been very useful for getting information on ionization density at the Bragg peak (Raju et al., 1967).

V. TECHNIQUES OF EXPOSURE

A. THE TRACK-AVERAGE AND TRACK-SEGMENT TECHNIQUES

It has long been known that the radiobiological effects depend on the specific energy loss of the particles in the biological samples (Lea, 1946; Timofeeff-Ressovsky and Zimmer, 1947; Zirkle, 1952). Two methods have been used extensively to obtain variations of the specific energy loss in the biological test objects, namely the track-average method and the track-segment method.

The track-average method applies when the thickness of the biological object in question is large compared to the particle penetration or if random portions of different tracks pass through the object. This results in a wide spread in LET values ranging from that characteristic of the lowest energy particles used to a minimum value determined by the charge and maximum velocity of the particles in the sample. The heterogeneity of the specific energy-loss values becomes even more pronounced if there is a nonuniformity of the initial particle energy or if several kinds of particles and rays are involved, as in a neutron beam.

The track-segment method, on the other hand, applies when the thickness of the biological sample is small compared to the range of a parallel monoenergetic particle beam. The technique is to place the samples along the particle path at a point where the LET has been predetermined. Different LET values are obtained in separate experiments by utilizing different linear portions of the particle track in successive experiments. Another possibility is to prepare a stack of

thin samples sandwiched between thin absorbers so that the total stack is thick enough to stop the particle beam. By analyzing separately the biological effects that are induced in each sandwich and that result from one single exposure, one can study the effects of varying specific energy loss over the entire range attainable by the radiation in question (Pollard et al., 1955). The method enables one to obtain relatively narrow distributions of LET in each sample. The disadvantage, however, is that with a given monoenergetic beam the greatest variations in mean energy loss attained in this way are usually only about one order of magnitude.

With the availability of heavy-ion linear accelerators that can produce monoenergetic beams of stripped nuclei up through atomic number 18 with energies of 10 MeV/amu, different specific energy-loss values can be obtained in separate experiments by irradiating thin samples with particles of different atomic number but equal velocity. This method has the advantage that the range of energy-loss values can be extended to cover more than 3 orders of magnitude. Furthermore, the fraction of the total energy deposition in the samples due to delta rays is the same irrespective of the nuclei used, and the spectral distribution of the energy-loss values of the delta-ray component is identical for different beams of equal particle velocity (Howard-Flanders, 1958; Haynes and Dolphin, 1959). Nearly half the energy of the heavy ion is transferred to electrons which are capable of further ionization. When this ionization occurs outside the main heavy-ion track, the LET in the particle track is considerably less than the energy

loss of the heavy ion (LET_{∞}). These features have been of some help in evaluating the relationship between radiation-induced biological damage and the specific energy loss.

B. RIDGE FILTERS

For many applications it is desirable to modify the depth-dose distribution of heavy-charged-particle beams. This can be done by the superposition of beams with differing depths of penetration. The relative intensity distribution of the various beams will determine the depth-dose distribution obtained. Sometimes it is desirable to produce a modified depth-dose distribution in a single exposure; many variations in depth-dose distribution may be obtained by use of a composite absorber, called a "ridge filter" (Karlsson, 1964). This filter is composed of a series of repeating units placed side by side to form a composite absorber whose cross section is larger than the beam area. Each unit is essentially a step-wise variable-thickness copper absorber. The width of an individual step determines the relative intensity, and the total thickness of the step determines the residual energy. The entire filter is oscillated on a line perpendicular both to the beam axis and to the length of the individual units of the ridge filter.

Figure 24 shows the depth-dose distribution of 187-MeV protons together with the modified depth-dose distribution and the ridge filter used for this modification. Such a modified depth-dose distribution is useful for uniform irradiation of a large volume.

The depth-dose distribution resulting from solar flare exposure generally decreases exponentially with depth. The depth-dose distribution of monoenergetic charged particles, on the other hand, increases with depth. However, it is possible to obtain the exponentially decreasing depth-dose distribution from monoenergetic charged-particle

beams by using an appropriate ridge filter. Figure 25 shows the depth-dose distribution of a degraded monoenergetic 910-MeV helium-ion beam, together with the modified depth-dose distribution and the ridge filter used for this modification.

C. DISCRETE LESIONS

Various discrete lesions can be produced for experimental purposes in animal tissue or for therapeutic purposes in man by use of collimated narrow beams of high-energy charged particles. By means of the Bragg peak of such beams, laminar lesion can be formed in a plane perpendicular to the beam direction at a depth determined by the range of the particles (Janssen et al., 1962; Malis et al., 1957). This technique as illustrated in Fig. 26 (Tobias, 1962) might be used to study the connections and functions of cerebral cortex (Malis et al., 1962). As the entrance dose is increased the lesion will be extended towards the surface. The cross section of these lesions is determined by the size and shape of the beam-defining aperture. Very large doses will produce lesions which will extend all the way along the path of the beam (Van Dyke and Janssen, 1963). If the aperture is a narrow slit, the resulting lesion will be knife-edged (Van Dyke et al., 1962).

The shape of these lesions can be further modified by rotating the object during irradiation. In this manner, it is possible to make spherical, elliptical, or disk-shaped lesions at various depths (Leksell et al., 1960; Tobias, 1962). Small spherical lesions are most easily produced by rotating the irradiated object 180 degrees about an axis at right angles to the beam direction, and using the plateau portion of the heavy-charged-particle beam with a circular cross section. Isodose contours for such an irradiation are shown in Fig. 27. The most significant contours may be made more nearly spherical by using an elliptical aperture with its major axis parallel to the axis of rotation.

The production of such lesions has been utilized in the treatment of Parkinson's disease (Tym et al., 1965).

Lesions of a more general form (ellipsoid) can be produced by rotation simultaneously about two perpendicular axes both of which are perpendicular to the beam axis. Isodose contours for such an irradiation are shown in Fig. 28. Such a technique has been in routine use at the 184-inch synchrocylotron in Berkeley for the suppression of pituitary function (Lawrence and Tobias, 1965).

ACKNOWLEDGMENTS

The authors are grateful to H. Bischsel for helpful suggestions, and to A. M. Koehler for helpful discussions and for his permission to use unpublished material. The authors take pleasure in thanking H. Aceto, S. B. Curtis, J. Howard, D. D. Love, H. D. Maccabee, P. W. Todd, and G. P. Welch for helpful suggestions.

FOOTNOTES AND REFERENCES

1 The authors work was generously supported by the U. S. Atomic Energy Commission, National Aeronautics and Space Administration, and Office of Naval Research.

* Southwest Center for Advanced Studies, Dallas, Texas, and guest scientist at Lawrence Radiation Laboratory, Berkeley.

† Norsk Hydro's Institute for Cancer Research, the Norwegian Radium Hospital, Montebello, Oslo 3, Norway.

Aamodt, R. L., Peterson, V., and Phillips, R. (1952). C^{12} (p, pn) C^{11} cross section from threshold to 340 MeV. Phys. Rev. 88, 739.

Barendsen, G. W., Walter, H. M. D., Fowler, J. F. and Bewley, D. K. (1963) Effects of Different Ionizing Radiations on Human Cells in Tissue Culture. III Experiments with Cyclotron-Accelerated Alpha-Particles and Deuterons. Rad. Res. 18, 106 (1963).

Barkas, W. H., and Berger, M. J. (1964). Tables of energy losses and ranges of heavy charged particles. In "Studies in penetration of charged particles in matter." NAS-NRC 1133.

Bethe, H. and Ashkin, J. (1953). Passage of heavy particles through matter. In "Experimental Nuclear Physics," Wiley and Sons, Inc. (E. Segre. ed.) Vol. 1, 166.

Bichsel, H., Mozley, R. F., and Avon, W. A., Range of 6 to 18 MeV protons in Be, Al, Cu, Ag and Au. Phys. Rev. 105, 1788.

Bichsel, H., and Uehling, E. A. (1960). Multiple scattering correction for proton ranges and the evaluation of the L-shell correction and I value for aluminum. Phys. Rev. 119, 1670.

Bichsel, H. (1963). Passage of charged particles through matter. In "American Institute of Physics Handbook" (D. E. Gray et al., eds.) 2nd ed., p. 8-20, McGraw-Hill, New York.

Bichsel, H. (1967). A Fortran program for the calculation of the energy loss of heavy charged particles. Lawrence Radiation Laboratory Report UCRL-17538.

Birge, A. C. and Sayeg, J. A. (1959). The effects of accelerated carbon nuclei and other radiations on the survival of haploid yeast. Rad. Res. 10, 433.

Blosser, T. V., Malienschein, F. C., and Freestone, R. M., Jr; (1964). The energy deposition in a water-filled spherical phantom by secondaries from high-energy protons and by neutrons. Health Phys. 10, 743.

Bobkov, V. G., Demin, V. P., Keirim-Markus, I. B., Kovalev, E. E., Larichiv, A. V., Sakovich, V. A., Smirennyy, L. N., Sychkov, M. A., (1964). "Radiation Safety During Space Flights." NASA Technical Translations, NASA-TT-F-356.

Born, J. L., Anderson, A. O., Anger, H. O., Birge, A. C., Blanquet, P., Brustad, T., Carlson, R. A., Van Dyke, D. C., Fluke, D. J., Garcia, J., Henry, J. P., Knisely, R. M., Lawrence, J. H., Riggs, C. W., Thorell, B., Tobias, C. A., Toch, P., and Welch, G. P. (1959), Biological and medical studies with high-energy particle accelerators. Prog. Nucl. Ener. Series VII, Vol. 2, p. 189.

Brustad, T., and Fluke, D. J. (1958). Effect of stripped carbon and oxygen ions in lysozyme. Rad. Res. 9, 95.

Brustad, T., Ariotti, P., and Lyman, J. T. (1960). Experimental set-up and dosimetry for investigating biological effects of densely ionizing radiations. Lawrence Radiation Laboratory Report UCRL-9454.

Brustad, T., (1961). Molecular and cellular effects of fast charged particles. Rad. Res. 15, 139.

Chamberlain, O., Segre, E., and Weigand, C. (1951). Experiments on proton-proton scattering from 120 to 345 MeV. Phys. Rev. 83, 923.

Cumming, J. B. (1963). Monitor reactions for high energy proton beams. Ann. Rev. Nucl. Sci. 13, 26.

Dolphin, G. W., and Hutchinson, F. (1960). The actions of fast carbon and heavier ions on biological materials. I. The inactivations of dried enzymes. Rad. Res. 13, 403.

Engstron, A., and Lindstrom, B. (1958). "The Weighing of Cellular Structure by Ultra-soft x-rays. General Cytochemical Methods," (Danielli, J. F., ed.) Academic Press, New York, 1, p. 1.

Fano, U. (1963). Penetration of protons, α particles and mesons. Ann. Rev. Nucl. Sci. 13, 1; reprinted in NAS-NRC 1133 (1964).

Fleischer, R. L., Price, P. B., and Walker, R. M., (1965). Tracks of charged particles in solids. Science 149, 383.

Fowler, P. H., and Perkins, D. H. (1961). Possibility of therapeutic applications of beams of negative π-mesons. Nature 189, 524.

Gooding, T. J., and Eisberg, R. M. (1957). Statistical fluctuations in energy losses of 37-MeV protons. Phys. Rev. 105, 357.

Gordon, H.S., and Behman, G.A. (1963). Particle accelerators. In "American Institute of Physics Handbook," 2nd Ed., McGraw-Hill 8-168.

Goulding, F.S. (1965). "Semiconductor detectors for nuclear spectrometry." Lawrence Radiation Laboratory Report UCRL-16231.

Gray, L.H. (1961). Radiobiologic basis of oxygen as a modifying factor in radiation therapy. Am. J. Roentgenol. Radium Therapy Nucl. Med. 85, 803.

Grew, G. (1965). Cyclotron tests to determine the response of solid-state detectors to protons of energies 50 to 160 MeV for use in a proton spectrometer. IEEE Trans. NS-12 (1), 308.

Hanna, R.C., and Hodges, T.A. (1965). A differential ion chamber for beam energy measurement. Nucl. Instr. Methods 37, 346.

Haynes, R.H., and Dolphin, G.W. (1959). The calculation of linear energy transfer, with special reference to a 14 MeV electron beam and 10 MeV per nucleon ion beams. Phys. Med. Biol. 4, 148.

Heckman, H.H., Perkins, B.L., Simon, W.G., Smith, F.M., and Barkas, W.H. (1960). Ranges and energy-loss processes of heavy ions in emulsion. Phys. Rev. 117, 544.

Henrikson, T. (1966). Production of free radicals in solid biological substances by heavy ions. Rad. Res. 27, 676.

Howard-Flanders, P. (1958). Physical and chemical mechanisms in the injury of cells by ionizing radiations. Advances in Biol. Med. Phys. 8, 553.

Hubbard, E. L., and MacKenzie, K. R. (1952). The range of 18 MeV protons in aluminum. Phys. Rev. 85, 107.

Hubbard, E. L. (1961). Heavy ion accelerators. Ann. Rev. Nucl. Sci. 2, 419.

Hubbard, E. L., Baker, W. R., Ehlers, K. W., Gordon, H. S., Main, R. M., Norris, N. J., Peters, R., Smith, L., Van Alta, C. M., Voelker, F., Anderson, C. E., Beringer, R., Gluckstron, R. L., Knon, W. J., Malkin, M. S., Quinton, A. R., Scharcz, L., and Wheeler, G. W. (1961). Heavy-ion linear Accelerator, Rev. Sci. Instr. 32, 621.

Janni, J. F. (1966). "Calculations of energy loss, range, path length, straggling, multiple scattering, and the probability of inelastic nuclear collisions for 0.1-to 1000-MeV protons." Air Force Weapons Laboratory. AFWL-TR 65-150.

Jung, H. (1965). Effects of protons on enzymes. Work Shop Conference on Space Radiation Biology. Sept. 7-10, Univ. of Calif. Berkeley, Calif. Proceedings to be published by Radiation Research. Suppl 7.

ICRU Report 10a (1962). NBS Handbook 84 (1962). "Radiation quantities and units."

Janssen, P., Klatzo, I., Miquel, J., Brustad, T., Behar, A., Haymaker, W., Lyman, J. T., Henry, J., and Tobias, C. A. (1962). Pathologic changes in the brain from exposure to alpha particles from a 60 inch cyclotron. In "Response of the Nervous System to Ionizing Radiation" (Eds. Haley and Snider). Academic Press, p. 383.

Karlsson, B. G. (1964). Methoden zur Berechnung und Erzielung Einiger fur die Tiefentherapie mit Hochenergetischen Protonen gunstiger Dosisverteilungen. Strahlentherapie 124, 481.

Kjellberg, R. N., Koehler, A. M., Preston, W. M., and Sweet, W. H. (1962). Biological and clinical studies using Bragg peak of proton beam. 2nd International Congress of Radiation Research, Harrogate, Yorkshire, England.

Kjellberg, R. N., Koehler, A. M., Preston, W. M., and Sweet, W. H. (1964). Intracranial lesions made by the Bragg peak of a proton beam; in "Response of the Nervous System to Ionizing Radiation" (T. J. Haley and R. S. Snider, Eds.) Little, Brown and Company, Boston.

Koehler, A. M. (1965). Dosimetry of proton beams using small silicon diodes. Workshop conference on space radiobiology, Sept. 7-10, Univ. of Calif., Berkeley, Calif. (Proceedings to be published in Radiation Research) Suppl. 7.

Koehler, A. M. (1967). Private communication .

Landau, L. (1944). On the energy loss of fast particles by ionization. J. Phys. USSR 8, 201.

Larsson, B., Leksell, L., Rexed, B., Sourander, P., Mair, W., and Andersson, B. (1958). The high energy proton beam as a neurosurgical tool. Nature 182, 1222.

Larsson, B. (1961). Pre-therapeutic physical experiments with high energy protons. Brit. J. Radiol. XXXIV, 143.

Larsson, B., Leksell, L., and Rexed, B. (1962). The use of high energy protons for cerebral surgery in man. Acta Chir Scand. 125, 1.

Lawrence, J.H., and Tobias, C.A. (1965). Heavy particles in medicine. In "Progress in Atomic Medicine." Vol. 1. 127. (Edited by J.H. Lawrence) Greene and Stratton, New York.

Lea, D.E. (1946). "Actions of Radiation on Living Cells." Cambridge University Press.

Lea, D.E. (1955). "Action of Radiation on Living Cells." 2 ed. Cambridge University Press.

Leksell, L., Larsson, B., Andersson, B., Rexed, B., Sourander, P., and Mair, W. (1960). Lesions in the depth of the brain produced by a beam of high energy protons. Acta Radiol. 54, 251.

Lindhard, J. (1964). Thomas-Fermi approach and similarity in atomic collisions, In "Studies in Penetration of Charged Particles in Matter." NAS-NRC 1133.

Litton, G.M. (1966). Private communication.

Litton, G.M. (1967). Programme Bragg-a Fortran-IV program for calculating Bragg curves and flux distributions. Lawrence Radiation Laboratory Report UCRL-17391.

Litton, G.M., Wallace, R., and Tobias, C.A. (1967). Penetration of high energy heavy ions. Lawrence Radiation Laboratory Report UCRL-17292.

Lyman, J.T. (1965). Dark recovery of yeast following ionizing radiations. Ph.D. Thesis. Lawrence Radiation Laboratory Report UCRL-16030.

Maccabee, H. D., Raju, M. R., Tobias, C. A. (1966). Fluctuations of energy loss in semiconductor detectors. IEEE Trans. Nucl. Sci. NS-13, 176.

Maccabee, H. D. (1966). "Fluctuations of energy loss by heavy charged particles in matter." Ph. D. thesis. Lawrence Radiation Laboratory Report UCRL-16931.

Maccabee, H. D., and Raju, M. R. (1967). Ionization Fluctuations in Cells and Thin Dosimeters. First International Symposium on Biological Interpretation of Dose from Accelerator Produced Radiation, Berkeley, March 1967. (Proceedings to be published). Also Lawrence Radiation Laboratory Report UCRL-17465.

Malis, L. I., Loevinger, R., Kruger, L., and Rose, J. E. (1957). Production of laminar lesions in the cerebral cortex by heavy ionizing particles. Science 126, 302.

Malis, L. I., Rose, J. E., Kruger, L., and Baker, C. P. (1962). Production of laminar lesions in cerebral cortex by deuteron irradiation. In "Response of the Nervous Systems to Ionizing Radiation" (Eds. Haley and Snider), Academic Press, p. 359.

McMillan, E. M. (1959). Particle Accelerators, Exp. Nucl. Phys. Vol. III, 639.

Manney, T. R., Brustad, T., and Tobias, C. A. (1963). Effects of glycerol and amonia on the radiosensitivity of haploid yeasts to densely ionizing particles. Rad. Res. 18, 374.

Measday, D. F. (1966). The ^{12}C (p, pn) ^{11}C reaction from 50 to 160 MeV, Nucl. Phys. 78, 476.

Moliere, F. (1948). Zeits. f. Naturforschung 3a, 78.

Neary, G. J., Savage, J. R. K., Evans, H. J., and Whittle, J. (1963). Ultimate maximum values of the RBE of fast neutrons and γ rays for chromosome aberrations. Intern. J. Radiation Biol. 6, 127.

Nefedor, Y. G. (1965). Problems of Radiation Safety in Space Flights NASA-TT-F-353.

Norman, A. (1965). Thermal Spike Effects in Heavy Ion Tracks. Workshop Conference on Space Radiobiology, Sept. 7-10, University of California, Berkeley, California (proceedings to be published in Radiation Research) Suppl. 7.

Northcliffe, L. C. (1960). Energy loss and effective charge of heavy ions in aluminum. Phys. Rev. 120, 1744.

Northcliffe, L. C. (1964). Passage of heavy ions through matter, Ann. Rev. Nucl. Sci. 13, 67; reprinted in NAS-NRC 1133 (1964).

Palmieri, J. N., and Goloskie, R. (1964). Calibration of 30-cm Faraday cup. Rev. Sci. Instr. 35, 1023.

Pollard, E. (1953). Primary ionization as a test of molecular organization. Adv. Biol. Med. Phys. 3, 153.

Pollard, E. C., Guild, W. R., Hutchinson, F., and Setlow, R. B. (1955). The direct action of ionizing radiation on enzymes and antigens. Progr. Biophys. Piophys. Chem. V, 72.

Preston, W. M., and Kochler, A. M. (1967). The effects of scattering on small proton beams (to be published).

Powers, E. L., Lyman, J. T., and Tobias, C. A. (1967). Some Effects of Accelerated Charged Particles on Bacterial Spores (to be published).

Pruitt, J.S. (1966). Secondary electron trajectories in a Faraday cup magnetic field. Nucl. Instr. Methods 39, 329.

Raju, M.R. (1965). Heavy Particle Studies with Silicon Detectors. Workshop Conference on Space Radiobiology Conference, Sept. 7-10, University of California, Berkeley, California (proceedings to be published in Radiation Research) Suppl 7.

Raju, M.R. (1966). The use of miniature silicon diode as a radiation dose meter. Phys. Med. Biol. 11, 371.

Raju, M.R., Lampo, E.J., Curtis, S.B., Sperinde, J.M., and Richman, C. (1967). Lithium drifted silicon detector used as a pulse dosimeter. IEEE Trans. Nucl. Sci. NS-14 [1] 559.

Raju, M.R., Richman, C., and Curtis, S.B. (1967). "A review of the physical characteristics of pion beams." Lawrence Radiation Laboratory Report UCRL-17441. Presented at the first International Symposium on the Biological Interpretation of Dose from Accelerator Produced Radiation, Berkeley, March 13-16, 1967 (Proceedings to be published by the U.S. Atomic Energy Commission).

Richman, C., Aceto, H., Raju, M.R., and Schwartz, B. (1966). The radiotherapeutic possibilities of negative pions. Am. J. Roent. XCVI, 777.

Roll, P.G., and Steigert, F.E. (1960). Effective charge of heavy ions in various media. Phys. Rev. 120, 470.

Rosenzweig, W., and Rossi, H.H. (1963). NYO-10716, Columbia University, New York.

Rossi, B. (1952). "High-Energy Particles." Prentice-Hall, New York.

Santoro, R. T., and Peele, R. W. (1964). "Measurement of the intensity of the proton beam of the Harvard University synchrocyclotron for energy-spectral measurements of nuclear secondaries." ORNL-3505, Oak Ridge National Laboratory, Oak Ridge, Tenn.

Santoro, R. T. (1965). "The space, time and energy distribution of the proton beam of the Harvard University synchrocyclotron. ORNL-3722, Oak Ridge National Laboratory, Oak Ridge, Tenn.

Santoro, R. B., Bertrand, F. E., Love, T. A., and Peele, R. W. (1966). "Beam energy measurements at the Oak Ridge isochronous cyclotron." ORNL-TM-1382. Oak Ridge National Laboratory, Oak Ridge, Tenn.

Sargent, T. W. (1962). Metabolic studies with Fe^{59}, Ca^{47} and C^{11} in various diseases. Proceedings of the Symposium on Whole Body Counting Held by the International Atomic Energy Agency, Neue Hofburg, Vienna, June 12-16, 1961

Sayeg, J. A., Birge, A. C., Beam, C. A., and Tobias, C. A. (1959). The effects of accelerated carbon nuclei and other radiations on the survival of haploid yeast. II. Biological experiments, Rad. Res. 10, 449.

Schambra, P. E., Rauth, A. M., Northcliffe, L. C. (1960). Energy loss measurements for heavy ions in Mylar and polyethlyene. Phys. Rev. 120, 1758.

Scott, W. T. (1963). The theory of small-angle multiple scattering of fast charged particles. Rev. Mod. Phys. 35, 231.

Seltzer, S., and Berger, M. (1964). Energy loss straggling of protons and mesons: tabulation of Vavilov distribution. "Studies in Penetration of Charged Particles in Matter," NAS-NRC Pub. No. 1133 p. 187.

Slater, J. V., Lyman, J., Tobias, C. A., Amer, N. M., Bech, J. S., Beck, M., and Slater, A. J. (1964). Heavy ion localization of sensitive embryonic sites in Tribolium. Rad. Res. 21, 541.

Snyder, W. S., and Neufeld, J. (1957). On the Passage of Heavy Particles Through Tissue. Rad. Res. 6, 67.

Sperinde, J. M. (1967). Private communication.

Sternheimer, R. M. (1966). Density effect for the ionization loss of charged particles. Phys. Rev. 145, 247.

Steward, P. G. and Wallace, R. (1966). Calculation of stopping power and range energy values for any heavy ion in nongaseous media. Lawrence Radiation Laboratory Report UCRL-17314.

Steward, P. (1967). In Biomedical Studies with Heavy Ion Beams. Lawrence Radiation Laboratory Report UCRL-17357, p. 8.

Symon, K. R. (1952). Fluctuations in energy lost by high energy charged particles in passing through matter. Ph. D. thesis, Harvard University, 1948, summarized in High Energy Particles (1952). (B. Rossi). Prentice-Hall, New York p. 32.

Tautfest, G. W., and Fechter, H. R. (1955). A nonsaturable high-energy beam monitor. Rev. Sci. Instr. 26, 229.

Tilbury, R. S. (1966). "Activation analysis with charged particles." National Academy of Sciences, National Research Council Nuclear Science Series NAS-NRC 3110.

Timofeeff-Ressovsky, N. W., and Zimmer, K. G. (1947). "Das Trefferprinzip in der Biologie." Biophysik. Vol. 1, S. Hirzel, Leipzig.

Tobias, C. A., Anger, H. O., and Lawrence, J. H. (1952). Radiological use of high energy deuterons and alpha particles. Am. J. Roentgenol. Radium Therapy Nucl. Med. LXVII, 1.

Tobias, C. A., Roberts, J. E., Lawrence, J. H., Low-Beer, B. V. A., Anger, H. O., Born, J. L., McCombs, R., and Huggins, C. (1956). Irradiation Hypophysectomy and Related Studies Using 340 MeV Protons and 190 MeV Deuterons. International Conference in Peaceful Uses of Atomic Energy, Geneva, 1955. Proceedings (U. S. N. Y., 1956) 10, 95.

Tobias, C. A., Lawrence, J. H., Born, J. L., McCombs, R. K., Roberts, J. E., Anger, H. O. Low-Beer, B. V. A., and Huggins, C. B. (1958). Pituitary irradiation with high-energy proton beams--a preliminary report. Cancer Res. 18, 121.

Tobias, C. A. (1962). The use of accelerated heavy particles for production of radiolesions and stimulation in the central nervous system. In "Response of the Nervous System to Ionizing Radiation" (Eds. Haley and Snider) Academic Press, p. 325.

Tobias, C. A., and Todd, P. (1963). Analysis of the effects of high LET radiations on various strains of cells. Symposium on Biological Effects of Neutron Irradiations, Upton, N. Y., Oct. 1963. Biological Effects of Neutron and Proton Irradiation (IAEA, Vienna, 1964) 2, 410.

Tobias, C. A., and Manney, T. (1964). Some molecular and cellular effects of heavily ionizing radiations. Ann. N. Y. Acad. Sci. 114, 16.

Tobias, C. A., and Todd, P. (1967). Heavy charged particles in cancer therapy. Conference on Radiobiology and Radiotherapy, Colorado Springs, Colorado, Nov. 1-3 (1965). J. National Cancer Inst. Monograph 24, p. 1. (1967).

Trower, W. P. (1966). High-energy particle data. Vols. I-IV. Lawrence Radiation Laboratory Report UCRL-2426 Rev.

Turner, J. E., Zerby, C. D., Woodyard, R. L., Wright, H. A., Kinney, W. E., Snyder, W. S., and Neufeld, J. (1964). Calculation of radiation dose from protons to 400 MeV. Health Phys. 10, 783.

Tym, R., Lyman, J. T., Weyand, R. W., Tobias, C. A., Yanni, N. W., Born, J. L., and Lawrence, J. H. (1965). Heavy Particles and Parkinson's Disease. In "Donner Laboratory, Semi-Annual Report, Biology and Medicine," Lawrence Radiation Laboratory Report UCRL-16613, p. 104.

Van Allen, J. A. (1961). Corpuscular radiations in space. Rad. Res. 14, 540.

Van Dyke, D. C., Janssen, P., and Tobias, C. A. (1962). Fluorescein as a sensitive, semiquantitative indicator of injury following α-particle irradiation of the brain. In "Response of the Nervous System to Ionizing Radiation" (Eds., Haley and Snider) Academic Press, p. 369.

Van Dyke, D. C., Janssen, P. (1963). Removal of cerebral cortical tissue with negligible scar formation using a beam of high-energy particles. J. Neurosurgery 20, 289.

Vavilov, P. V. (1957). Ionization losses of high-energy heavy particles, ZH. Experim. I. Teor. F 12. [32] 920; English translation: Soviet Phys. JETP 5, 749.

Walker, R. (1965). Effect of massive charged particles. Workshop Conference on Space Radiobiology Sept. 7-10, University of California, Berkeley, California (Proceedings to be published in Radiation Research) Suppl 7.

Walske, M. C. (1952). The stopping power of κ-electrons. Phys. Rev. 88, 1283.

Walske, M. C. (1956). Stopping power of L-electrons. Phys. Rev. 101, 940.

Webber, W. R. (1963). "An evaluation of the radiation hazard due to solar-particle events." D2-90469. Aero Space Division, the Boeing Company, Seattle, Washington.

Webber, W. R. (1966). "An evaluation of solar-cosmic-ray events during solar minimum." D2-84274-1 Space Science Group, the Boeing Company, Seattle, Washington.

Welch, G. (1967). Private communication.

Whaling (1958). "The energy loss of charged particles in matter," Encyclopedia of Physics. Vol. XXXIV, p. 193.

Wheeler, R. V. (1966). Depth-dose for protons and pions from 1.0 to 10.0 BeV/c. Health Phys. 12, 653.

Williams, E. J. (1939). Concerning the scattering of fast electrons and of cosmic-ray particles. Proc. Roy. Soc. London 169, 531.

Williams, E. J. (1940). Multiple scattering of fast electrons and alpha-particles, and "curvature" of cloud tracers due to scattering. Phys. Rev. 58, 292.

Williamson, C. F., Boujot, J. P., and Picard, J. (1966). "Tables of range and stopping power of chemical elements for charged particles of energy 0.05 to 500 MeV." Rapport CEA-R3042, Centre D'Etudes Nucleaires De Saclay.

Wilson, R. R. (1946). Radiological use of fast protons. Radiology, 47, 487.

Zimmer, K. G. (1966). Some unusual topics in radiation biology. Rad. Res. 28, 830.

Zirkle, R. E. (1952). Speculations on cellular actions of radiations. In "Symposium on Radiobiology" (J. J. Nickson, Ed.) p. 333, Wiley, New York

Zirkle, R. E., and Tobias, C. A. (1953). Effects of ploidy and linear energy transfer on radiobiological survival curves. Arch. Biochem. Biophys. 47, 282.

Zirkle, R.E., and Bloom, W. (1953). Irradiation of parts of individual cells. Science 117, 487.

Zirkle, R.E. (1957). Partial cell irradiation. Adv. Biol. Med. Phys. 5, 103.

FIGURE LEGENDS

Fig. 1. Average residual energy of protons of initial energy 160 MeV as a function of thickness of water penetrated. It can be seen that the energy near the end of the range decreases much more rapidly than in the beginning.

Fig. 2. Stopping power of protons of energies from 20 keV to 10 BeV, in water and lead (data taken from Whaling, 1958, and Barkas and Berger, 1964). Arrows indicate the energy at which the stopping power is minimum. Dashed lines indicate values after density-effect correction for water. At energies below 80 keV, the stopping power decreases with decreasing energy. This is partly due to the reduction of effective charge. At intermediate kinetic energies, from 100 keV up to about 1 BeV, the energy region of interest for biomedical studies, the stopping power decreases with increasing energy, reaching a minimum near an energy equal to around twice the rest energy of the charged particle. At energies higher than 2 MC^2 (velocities of energetic protons close to the velocity of light), the term $-\log(1 - \beta^2)$ in B will cause the stopping power to increase with particle energy. A further correction is necessary for condensed materials. It is known as the density-effect correction and causes a reduction of S. It is discussed extensively by Sternheimer (1966).

Fig. 3. Number-distance curve showing the number of particles in a beam penetrating to a given depth. Projected range R_p and extrapolated range R_e.

Fig. 4. Theoretical range-energy and stopping power for various heavy ions in water (Steward, 1967).

Fig. 5. The calculated ratio of the standard deviation for protons, at depth T in a given material, relative to that at the end of the range R_0 (Preston and Koehler, 1967).

Fig. 6. Relative intensity (particles) of the beam as a function of distance from its central axis. The terms R_0 and R are the range and residual range, respectively. Absorption is neglected. The change is due to scattering alone (Sperinde, 1967).

a. 2-mm-diameter beam.

b. 20-mm-diameter beam.

Fig. 7. Calculated relative intensity (particles) I(x, 0, 0) on the axis of a uniform circular beam, of initial range R_0 = 12 cm of water and radius r_c at the collimator, as a function of water path x. Absorption is neglected; the change is due to scattering alone (Preston and Koehler, 1967).

Fig. 8. Relative dose on the axis of a uniform circular proton beam, of initial range R_0 = 12 cm of water and radius r_c at the collimator, as a function of water path x. The curve for $r_c = \infty$ is an experimental Bragg curve; the others are calculated (Preston and Koehler, 1967).

Fig. 9. Perspective view of large-volume and limited-volume ionization chambers.

Fig. 10. Block diagram of ionization chamber, integrating electrometer, amplifier, and high-voltage supply (HV).

Fig. 11. Faraday cup.

Fig. 12. Exploded view of a secondary emission monitor.

Fig. 13. Saturation curve for a secondary emission monitor.

Fig. 14. Experimental arrangement for measuring the Bragg curve.

Fig. 15. Central-axis depth-dose distribution of proton and helium-ion beams. The depth-dose distribution of high-energy proton beam (730 MeV) is different from the other curves. The initial dose build up is due to secondary particle production and the reduction of dose with depth is due to loss of particles through nuclear interaction (Refer to Sondhaus and Evans, Chap. 26).

Fig. 16. Bragg curves of Ne^{20}, O^{16}, C^{12}, and B^{11} ions of initial energy 10.4 ± 0.2 MeV/amu measured in aluminum but converted to tissue.

Fig. 17. Beam intensity as a function of position along a diameter of the beam, measured at 0 cm (a), 5.7 cm (b), 8.7 cm (c), and 11.4 cm (d) depth of penetration in water. The incident energy is 127 MeV and the mean end of range is at 11.4 cm depth.

Fig. 18. Data of Fig. 17 normalized to 100% intensity at maximum and plotted on a Gaussian scale.

Fig. 19. Isodose contours of a 910-MeV helium ion beam (degraded by 32 mm of copper) in water.

Fig. 20. Modified integral range curve for various heavy ions of initial energy 10.4 ± 0.2 MeV/amu. Since the Faraday cup measures the total charge of the beam, the ordinate represents the product of the number of particles and the average charge per particle.

Fig. 21. Modified integral range curve for 910-MeV helium-ion beam. This is very similar to the number-distance curve since the charge of these energetic ions remains essentially the same until the last few mg/cm^2 of the total range.

Fig. 22. Energy-loss probability, 730-MeV protons in 0.66-g/cm^2 silicon; k = 0.0338 (Maccabee et al., 1966).

Fig. 23. Energy distribution of charged particles at the Bragg peak (Raju, 1965).

Fig. 24. Depth-dose distribution of 187-MeV proton beam in water together with modified depth-dose distribution obtained by using ridge filter (redrawn from Karlson, 1964).

Fig. 25. Depth-dose distribution of degraded (1.5 inches of copper) 910-MeV helium-ion beam (large circles) together with modified depth-dose distribution obtained by using a ridge filter (small circles).

Fig. 26. Depth-dose distribution of heavy-charged-particle beam (upper left). On upper right is a hypothetical dose-effect relationship. Lower left shows the location and width of the laminar lesion effects greater than 50% are assumed to produce a lesion.

Fig. 27. Isodose contours for a small spherical lesion produced by a 910-MeV helium-ion beam collimated by a 6-mm diameter aperture and a 180-deg rotation used for the treatment of Parkinson's disease.

Fig. 28. Isodose contours for a small ellipsoidal lesion produced by a 910-MeV helium-ion beam, collimated by a (9.5 × 6.5 mm) aperture, used for pituitary suppression.

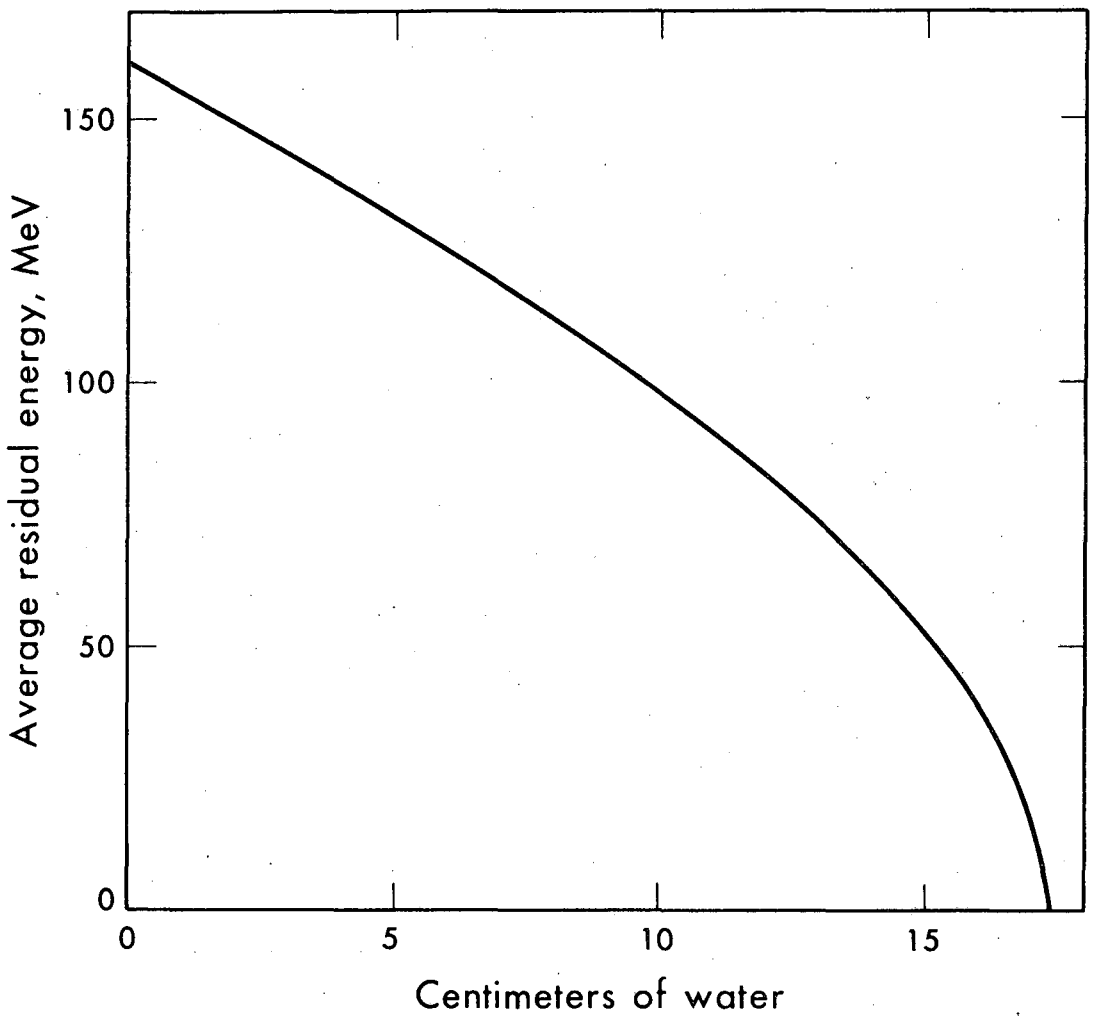

DBL 675-1625

Fig. 1.

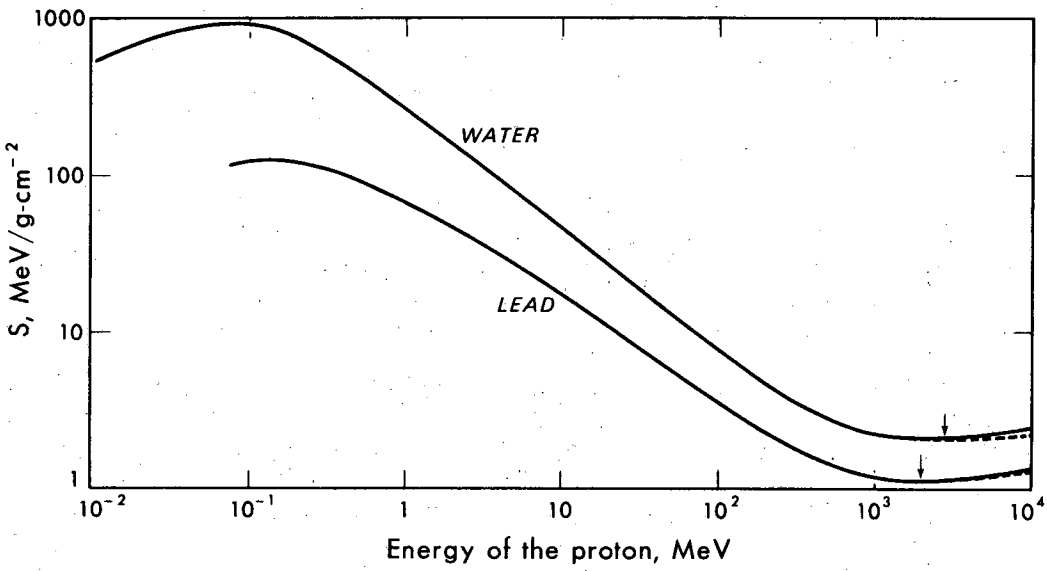

DBL 675-1626

Fig. 2.

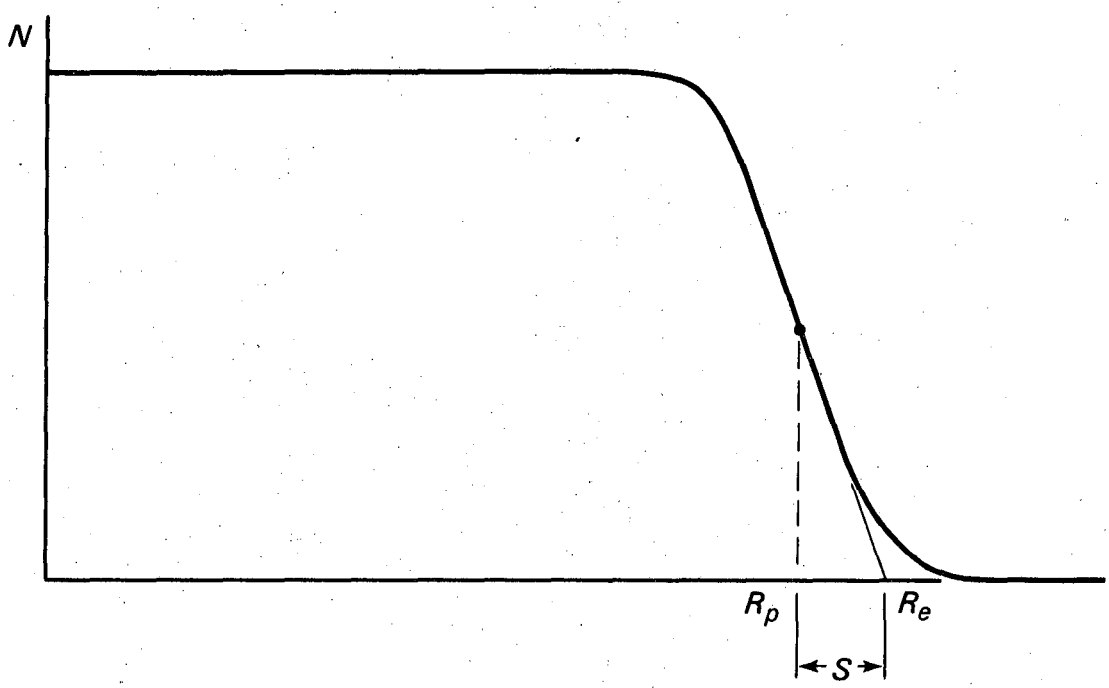

DBL 675-1627

Fig. 3.

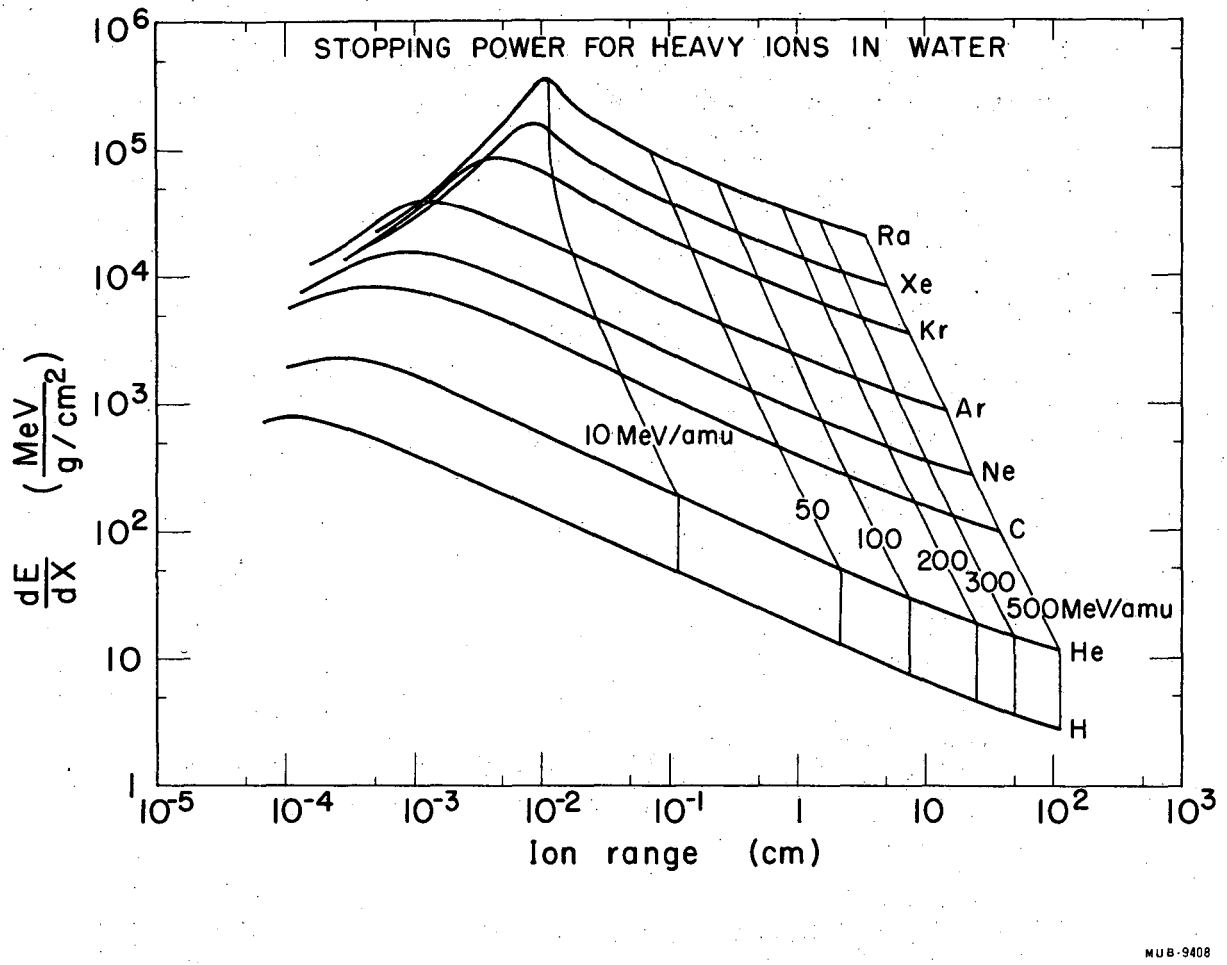
STOPPING POWER FOR HEAVY IONS IN WATER
dE/dX (MeV/g/cm²)
Ion range (cm)
Ra
Xe
Kr
Ar
Ne
C
He
H
10 MeV/amu
50
100
200
300
500 MeV/amu
MUB-9408

Fig. 4.

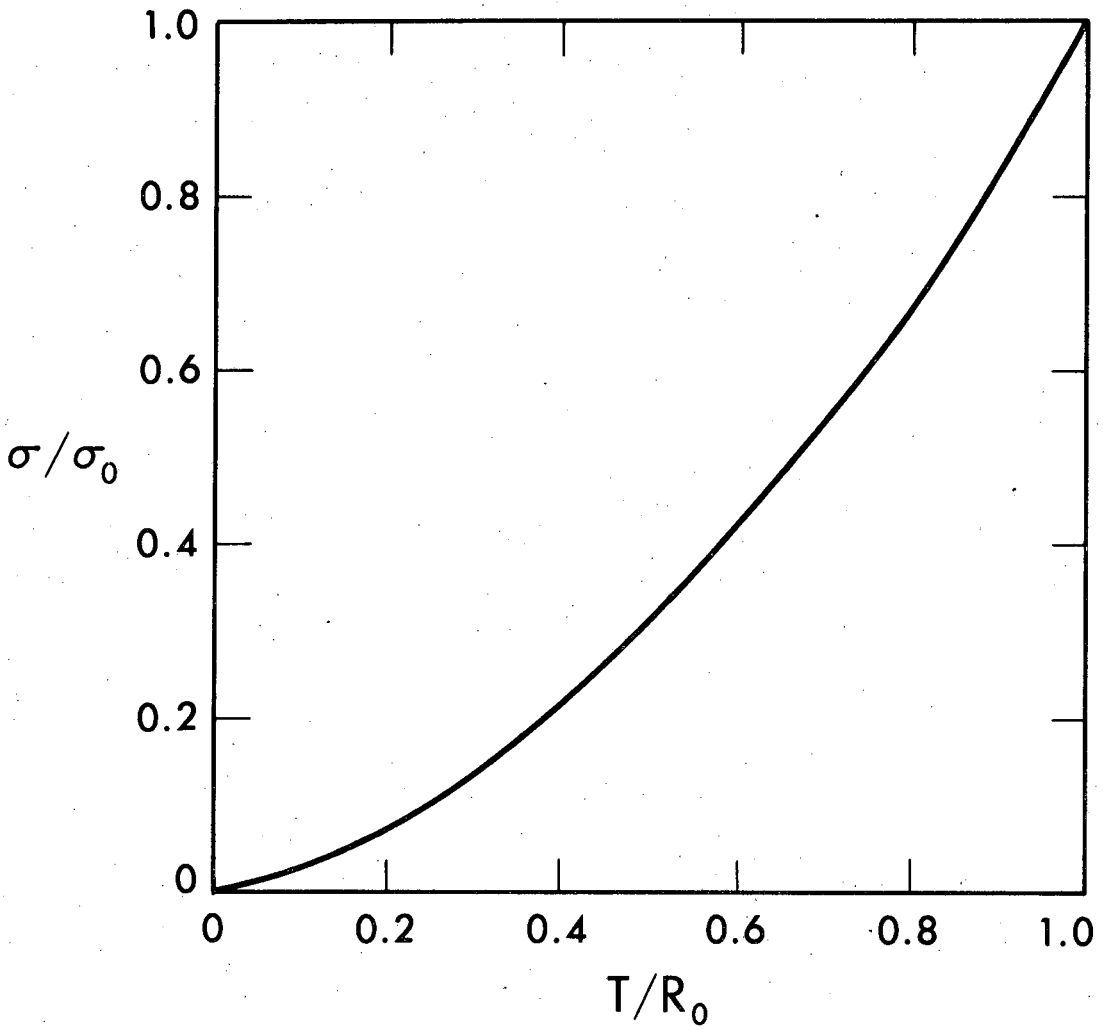

DBL 675-1628

Fig. 5.

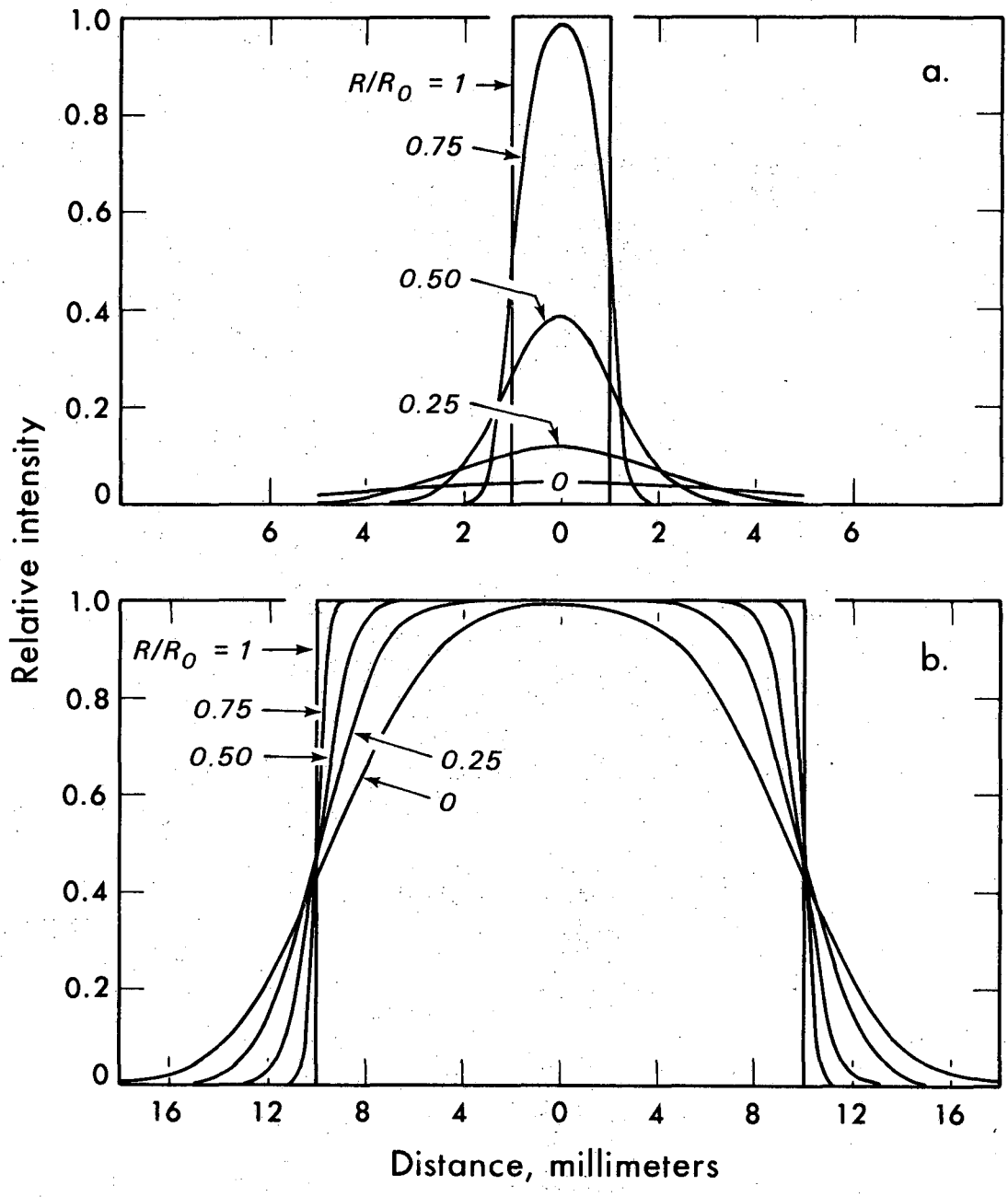

DBL 675-1629

Fig. 6.

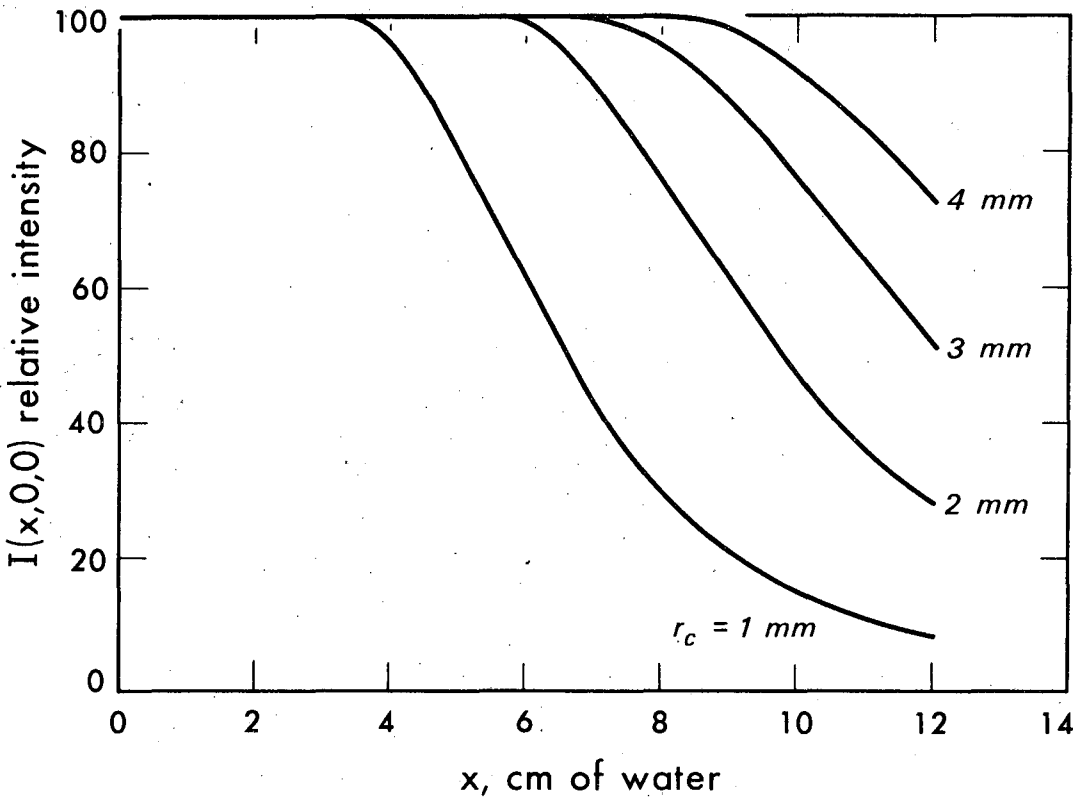

DBL 675-1630

Fig. 7.

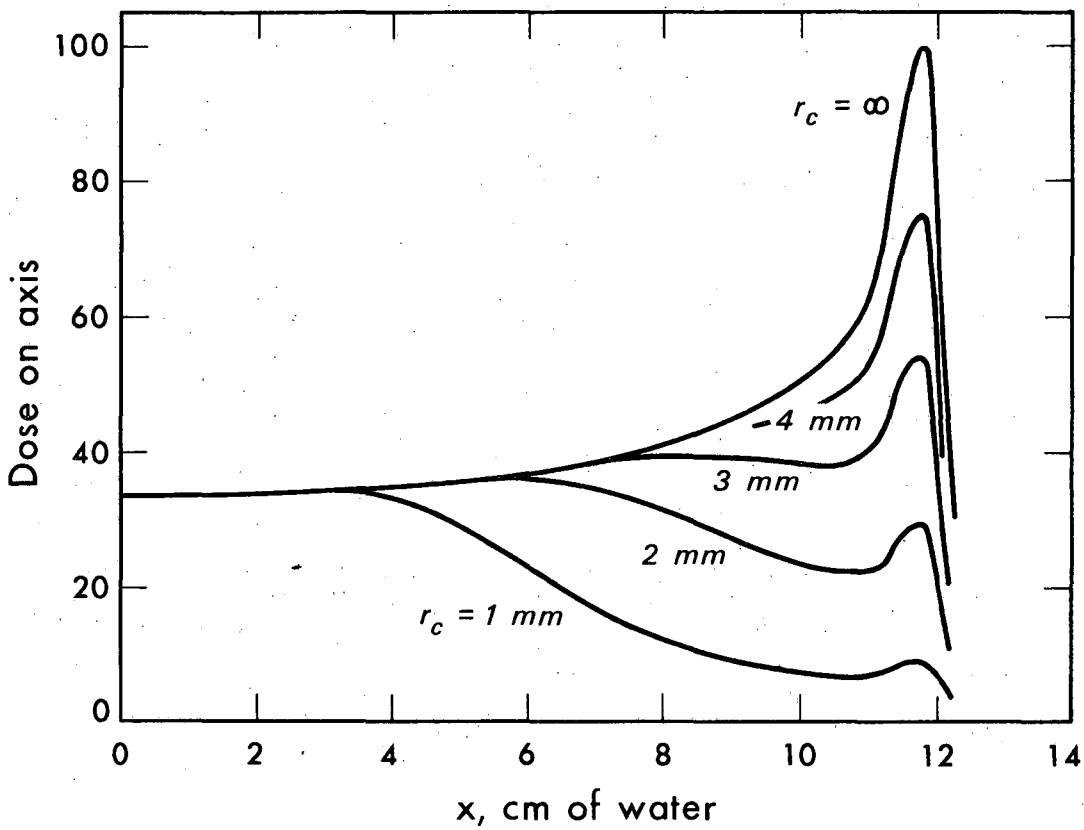

DBL 675-1631

Fig. 8.

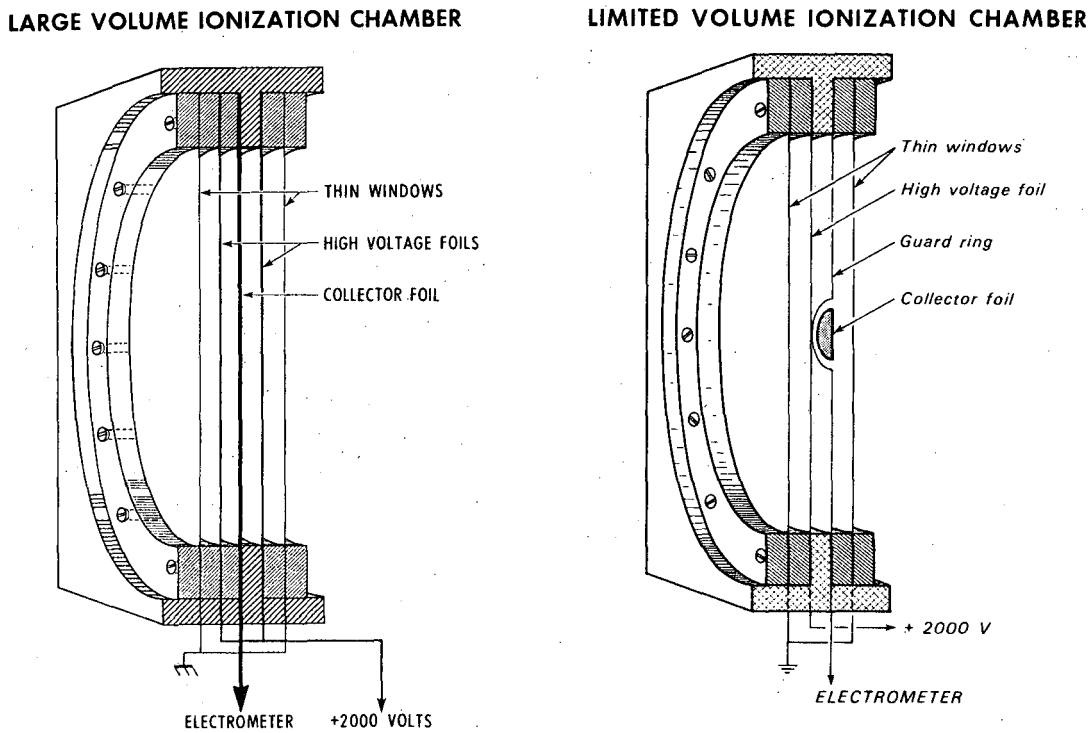

XBL 676-4128

Fig. 9.

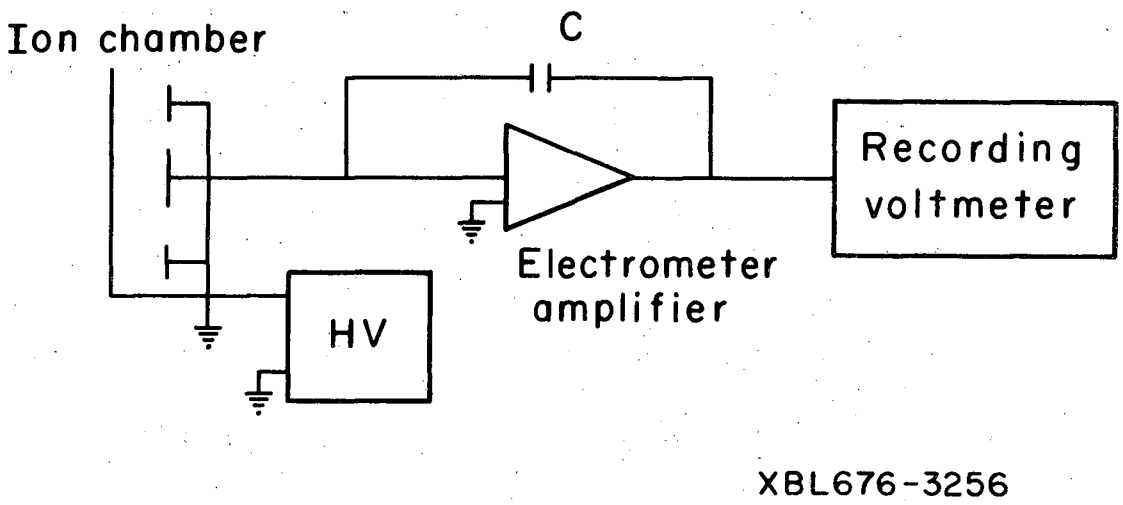
Ion chamber
C
Recording voltmeter
Electrometer amplifier
HV
XBL676-3256

Fig. 10.

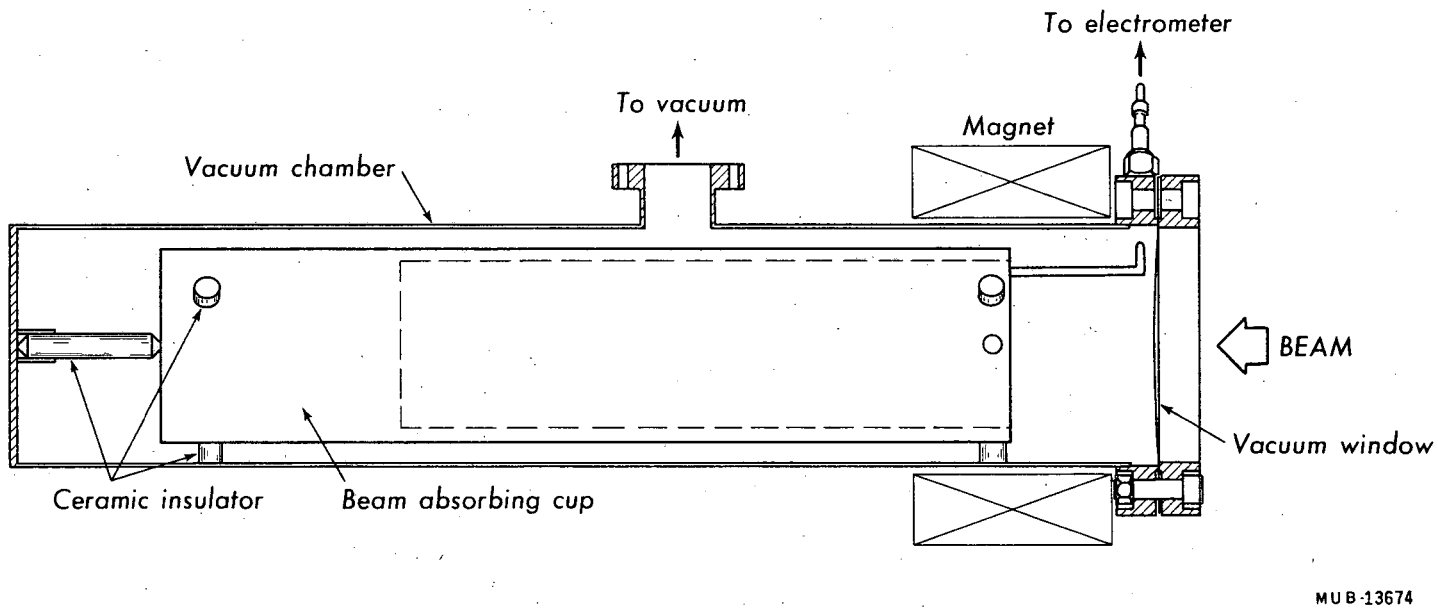
To electrometer
To vacuum
Magnet
Vacuum chamber
BEAM
Vacuum window
Ceramic insulator
Beam absorbing cup
MUB-13674

Fig. 11.

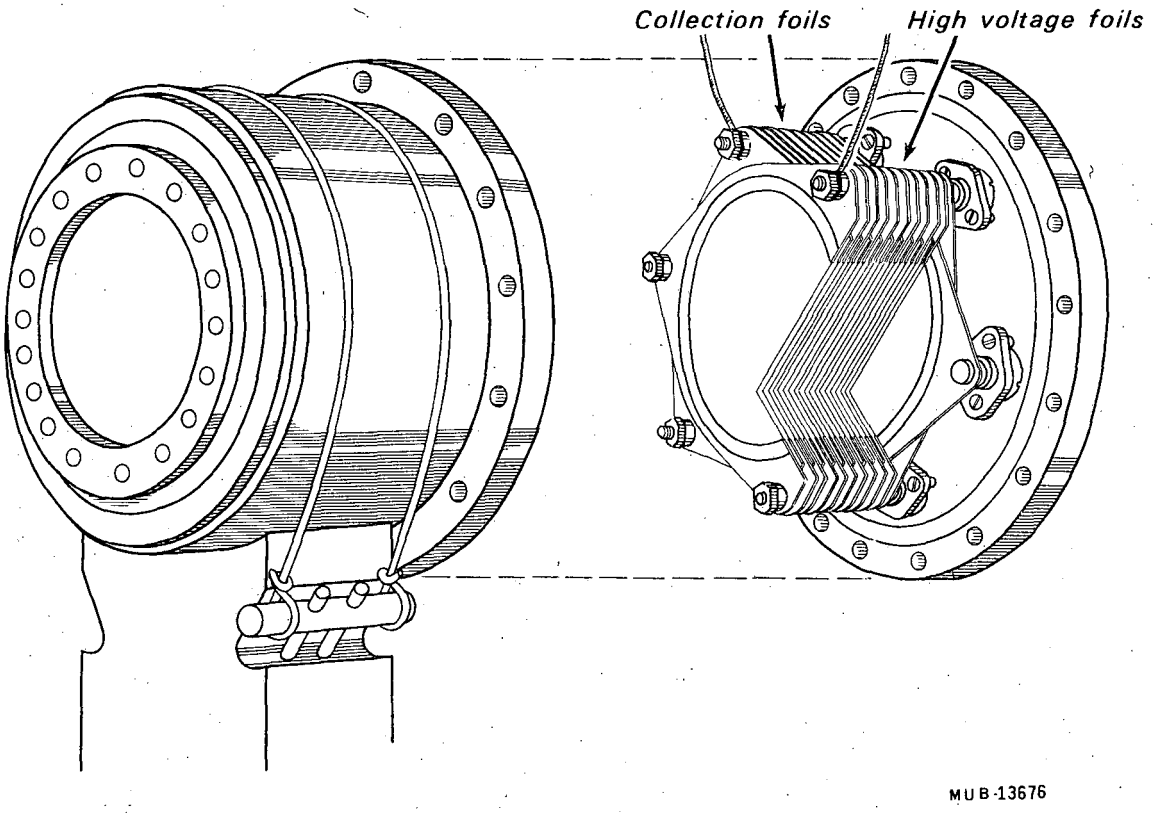

Fig. 12.

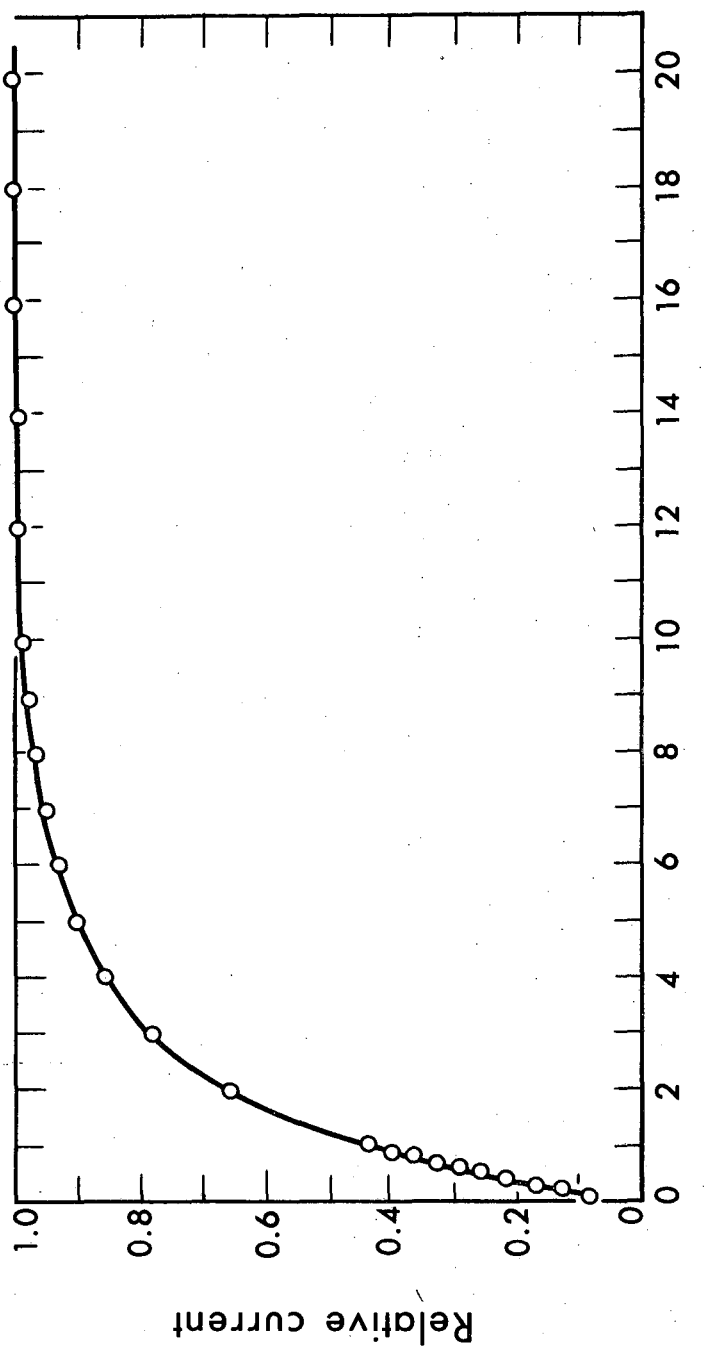

MUB-12975

Fig. 13.

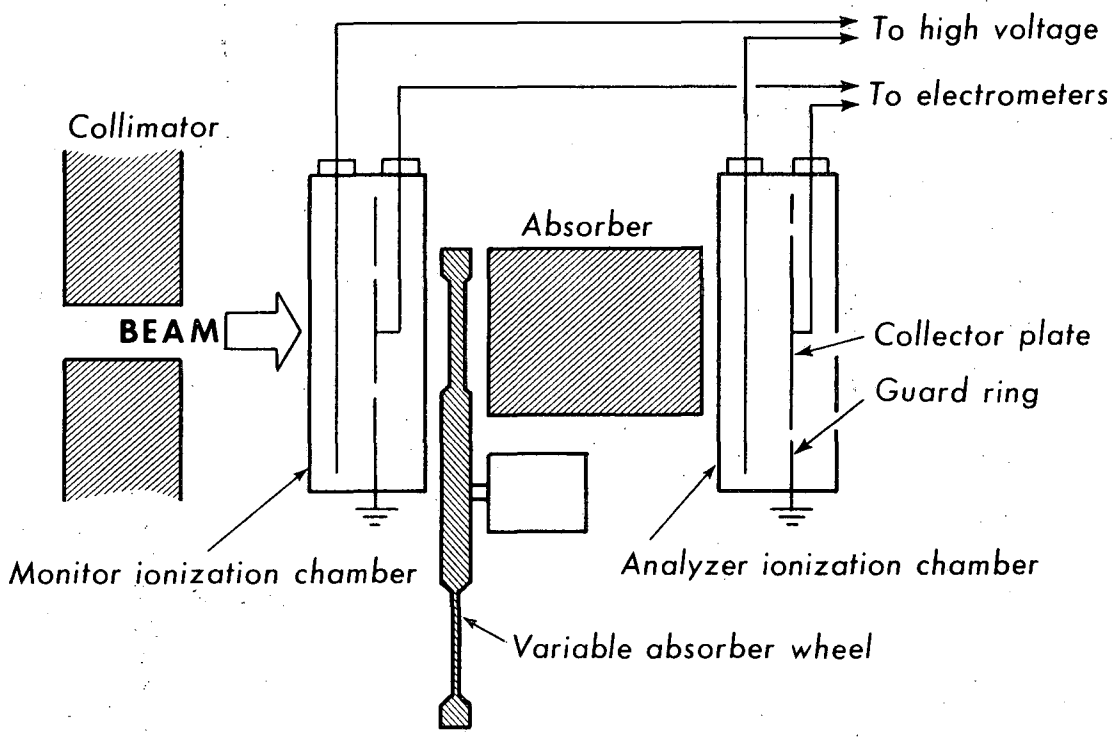
To high voltage
To electrometers
Collimator
Absorber
BEAM
Collector plate
Guard ring
Monitor ionization chamber
Analyzer ionization chamber
Variable absorber wheel
MUB-13671

Fig. 14.

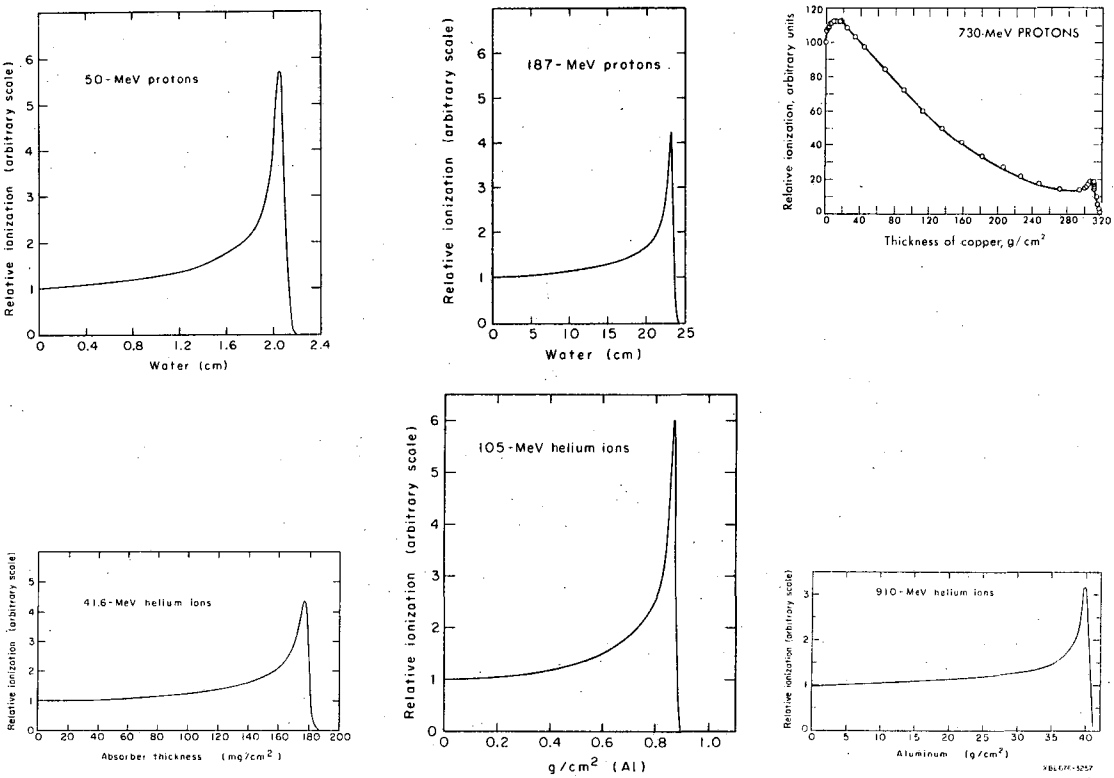

XBL 676-4131

Fig. 15.

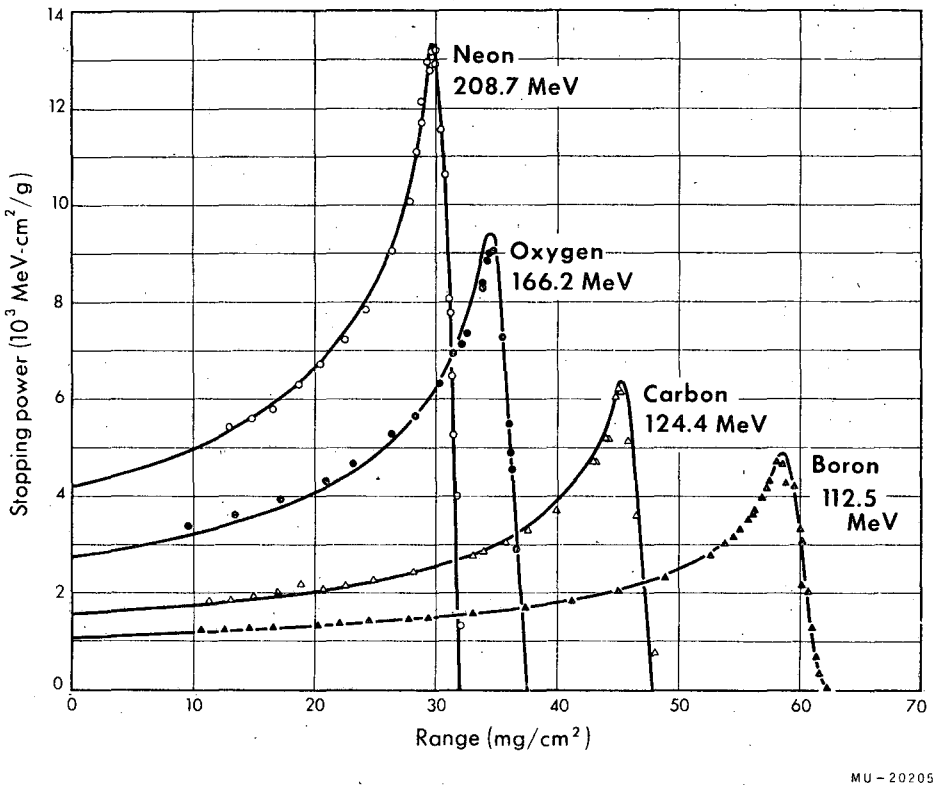
Neon
208.7 MeV
Oxygen
166.2 MeV
Carbon
124.4 MeV
Boron
112.5
MeV
Stopping power (10^3 MeV·cm^2/g)
Range (mg/cm^2)
0
2
4
6
8
10
12
14
0
10
20
30
40
50
60
70
MU-20205

Fig. 16.

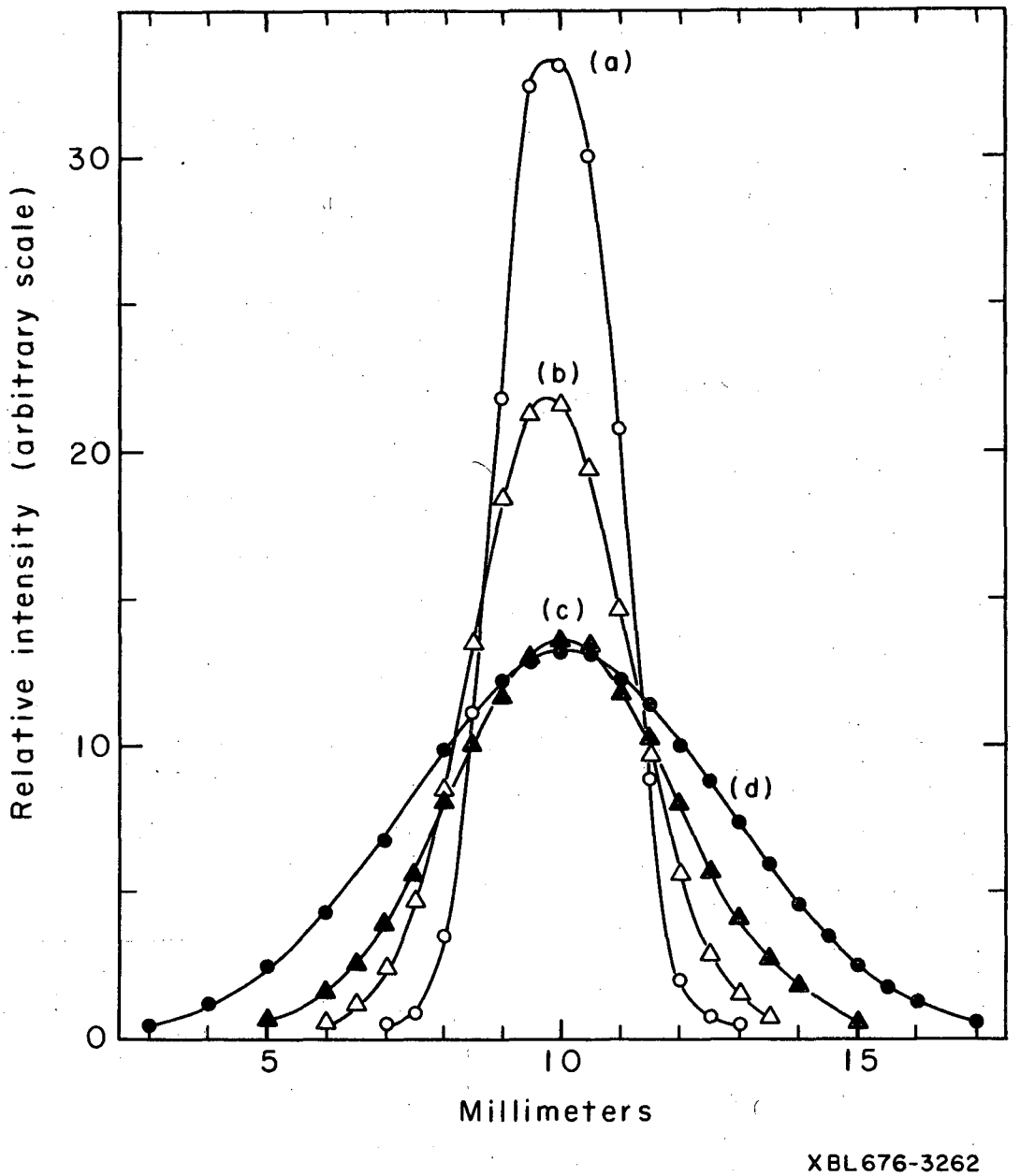
(a)
(b)
(c)
(d)
30
20
10
0
5
10
15
Relative intensity (arbitrary scale)
Millimeters
XBL676-3262

Fig. 17.

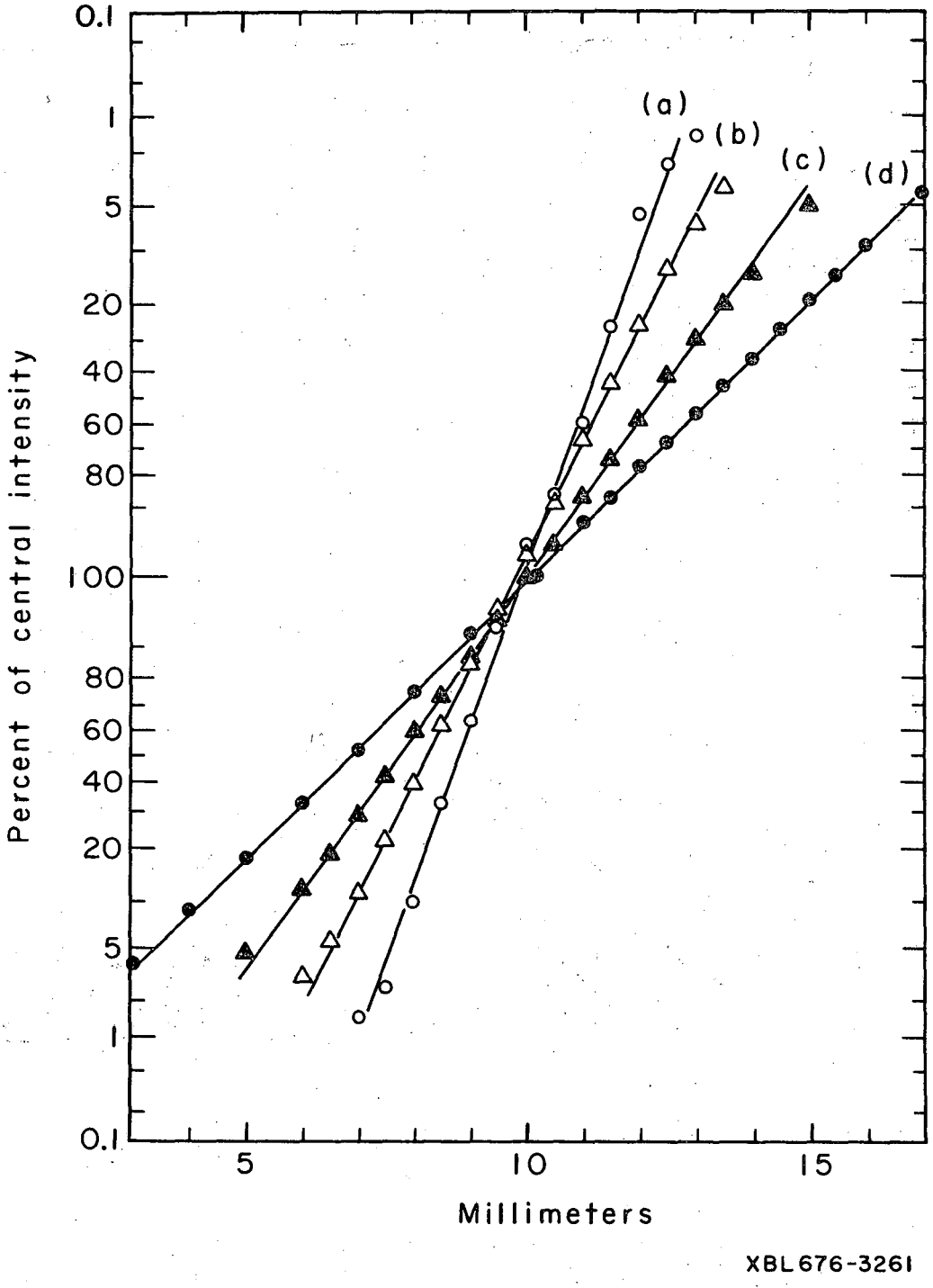
0.1
1
5
20
40
60
80
100
80
60
40
20
5
1
0.1
(a)
(b)
(c)
(d)
Percent of central intensity
5
10
15
Millimeters
XBL676-3261

Fig. 18.

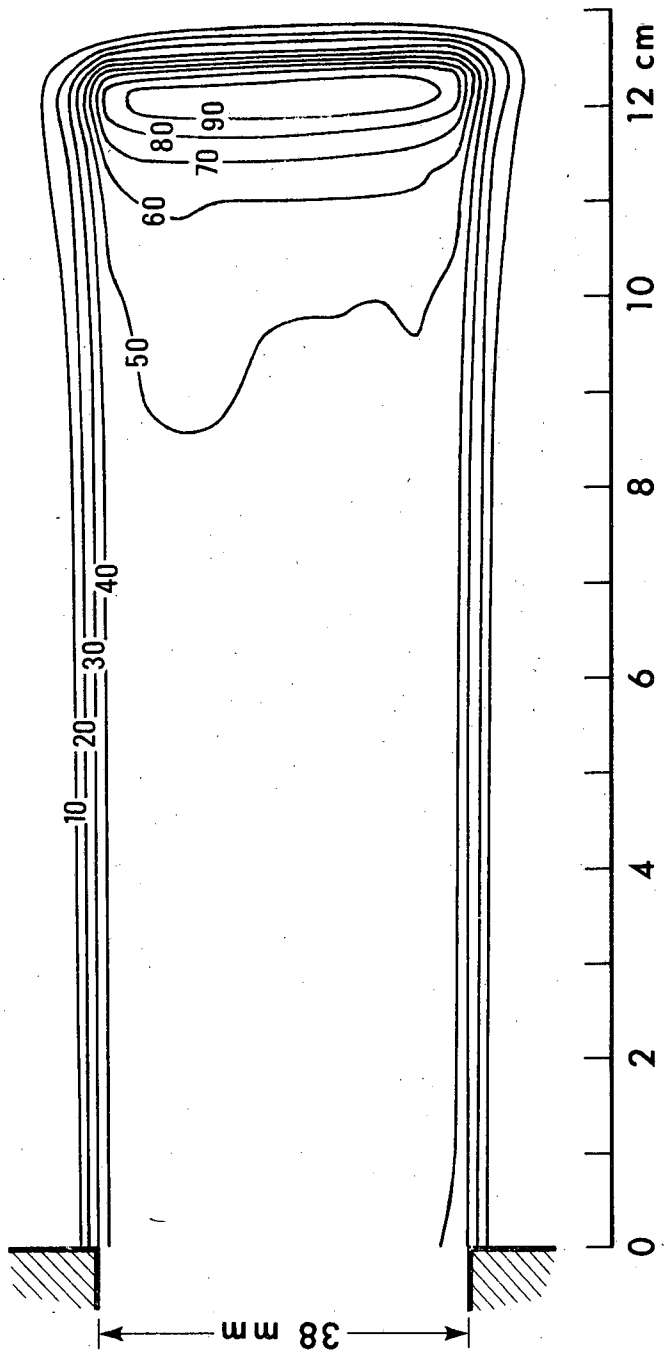

DBL 678-1717

Fig. 19.

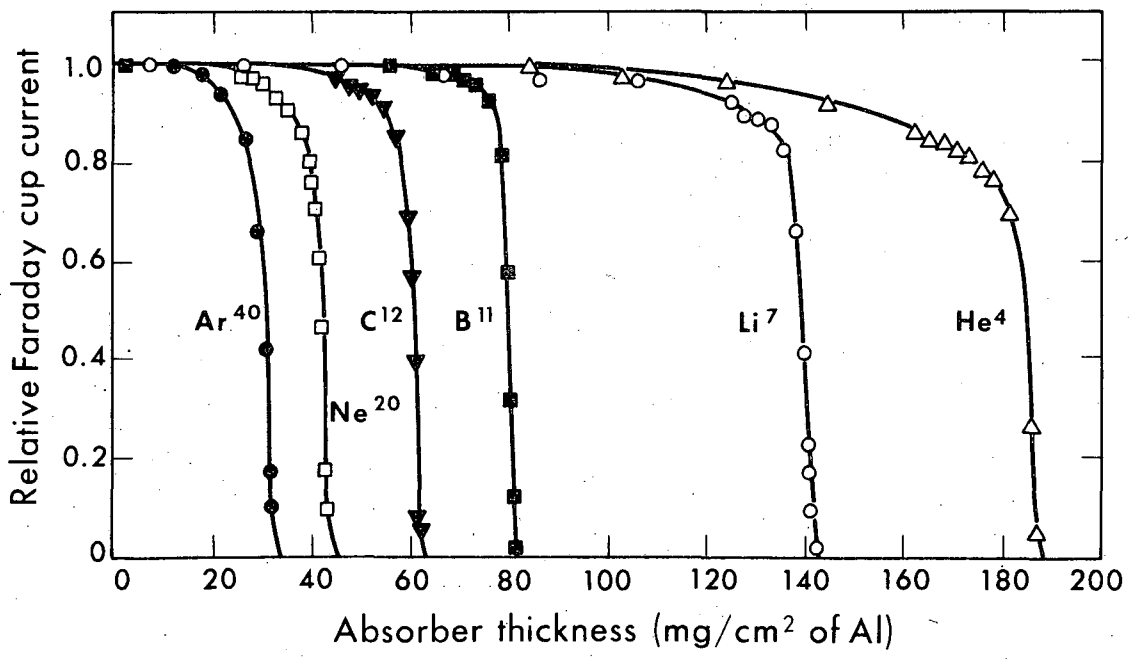

MU-35509

Fig. 20.

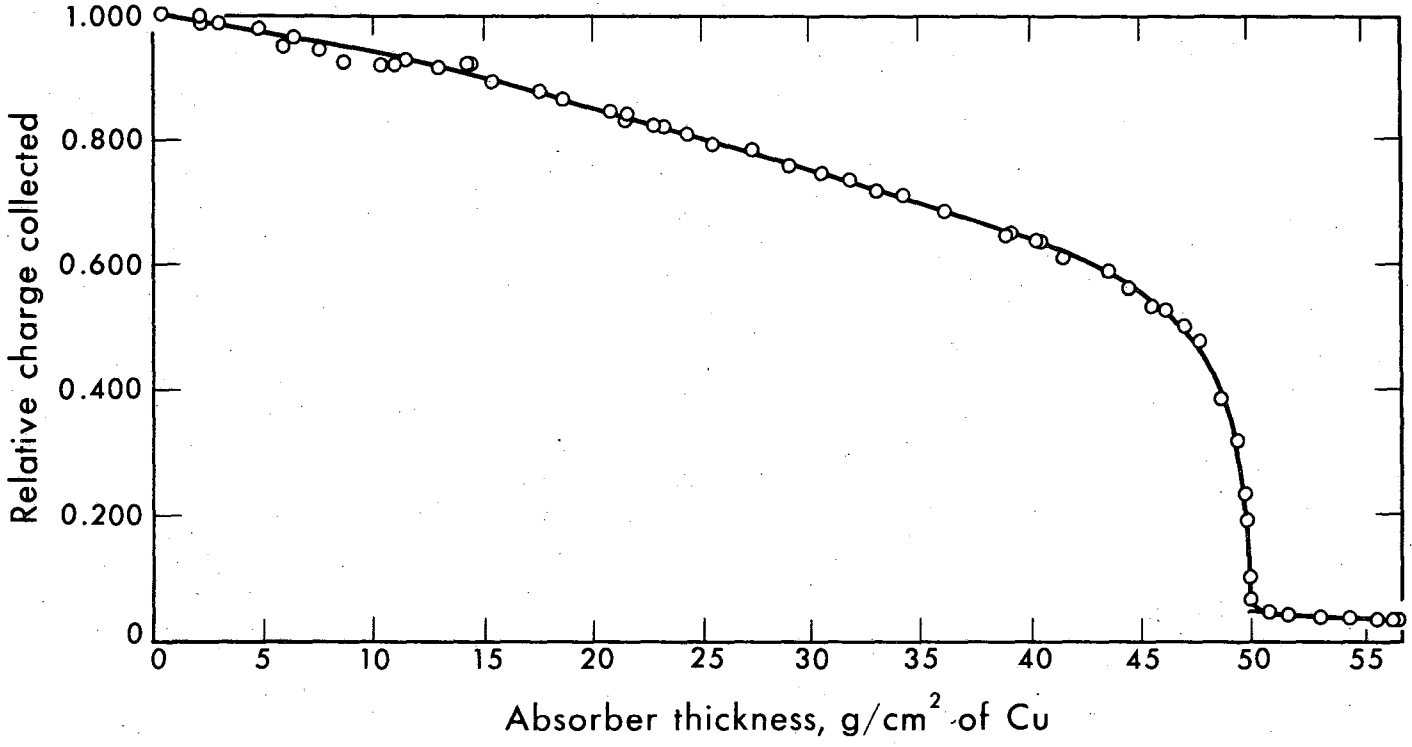

Fig. 21.

MUB-12977

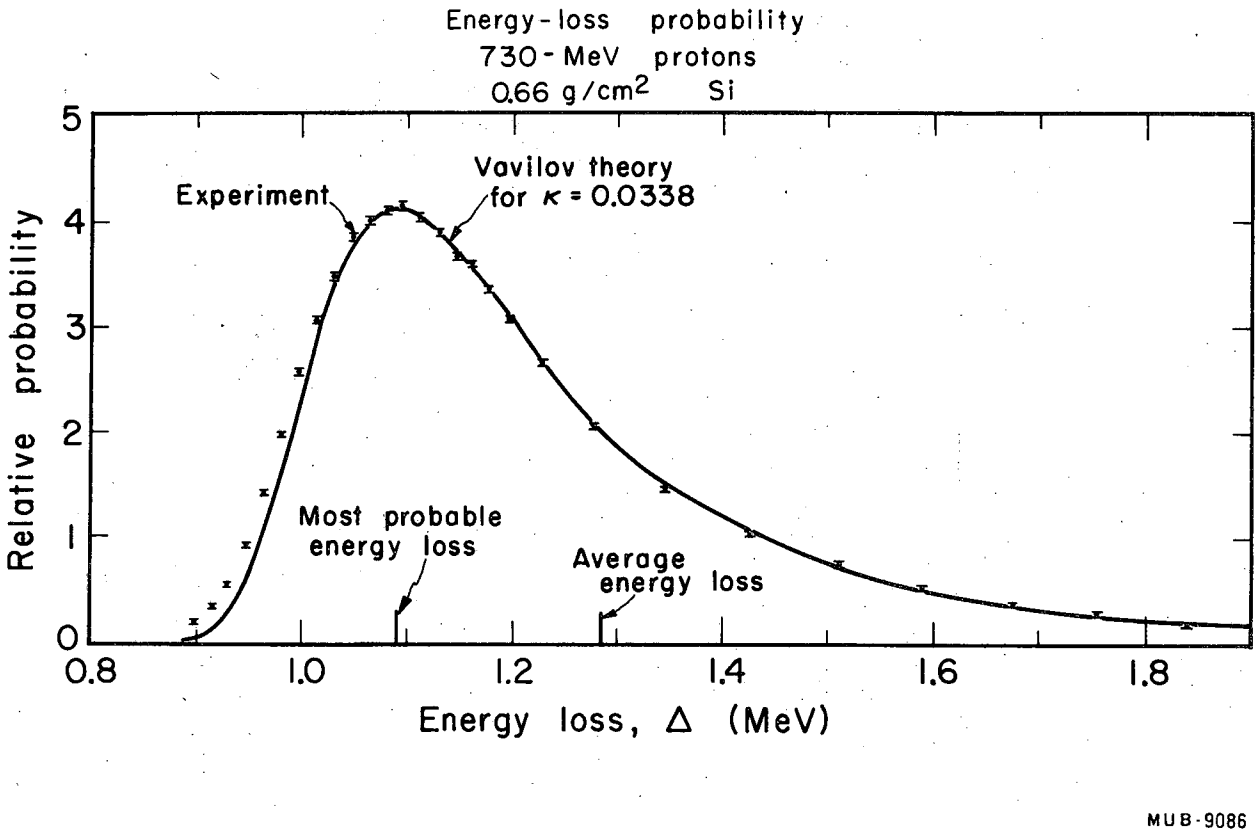
Energy-loss probability
730-MeV protons
0.66 g/cm2 Si
Experiment
Vavilov theory
for κ = 0.0338
Most probable
energy loss
Average
energy loss
Relative probability
Energy loss, Δ (MeV)
0
1
2
3
4
5
0.8
1.0
1.2
1.4
1.6
1.8
MUB-9086

Fig. 22.

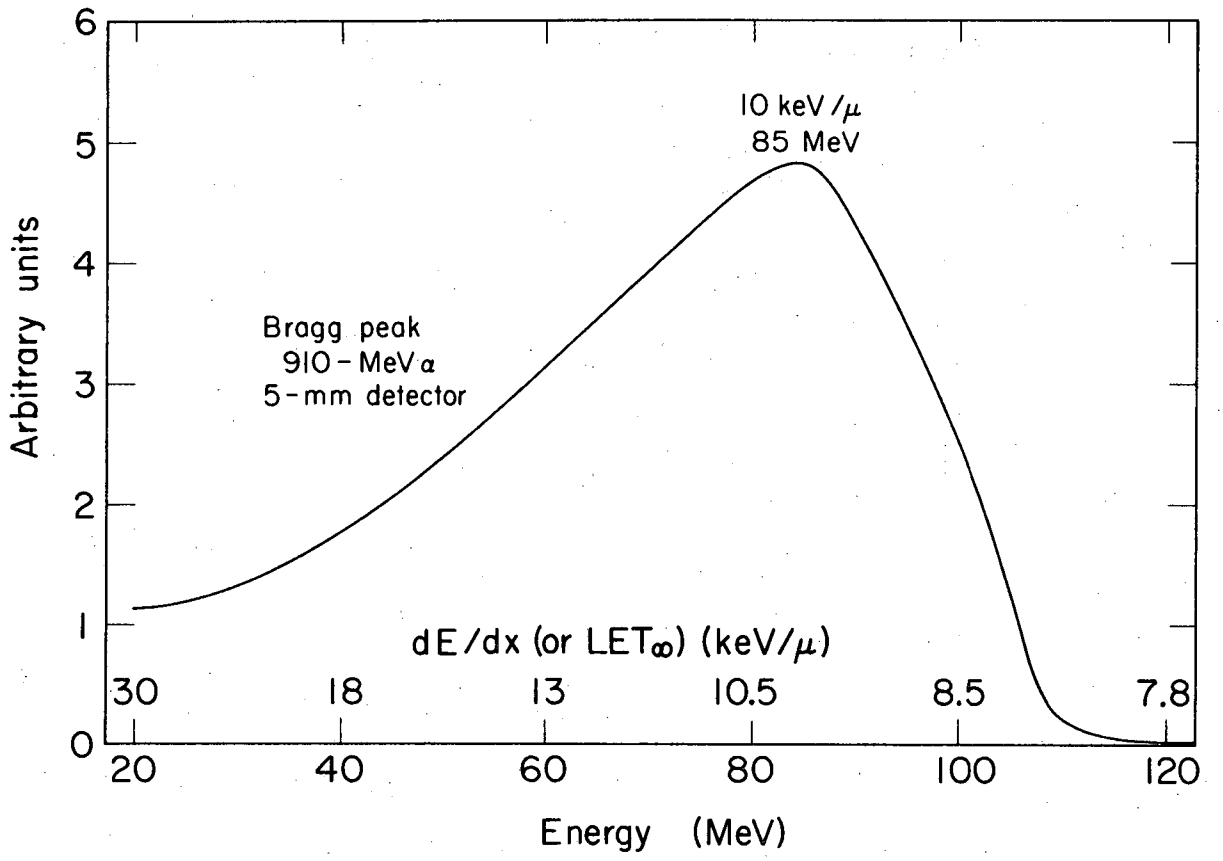

MUB-7543-A

Fig. 23.

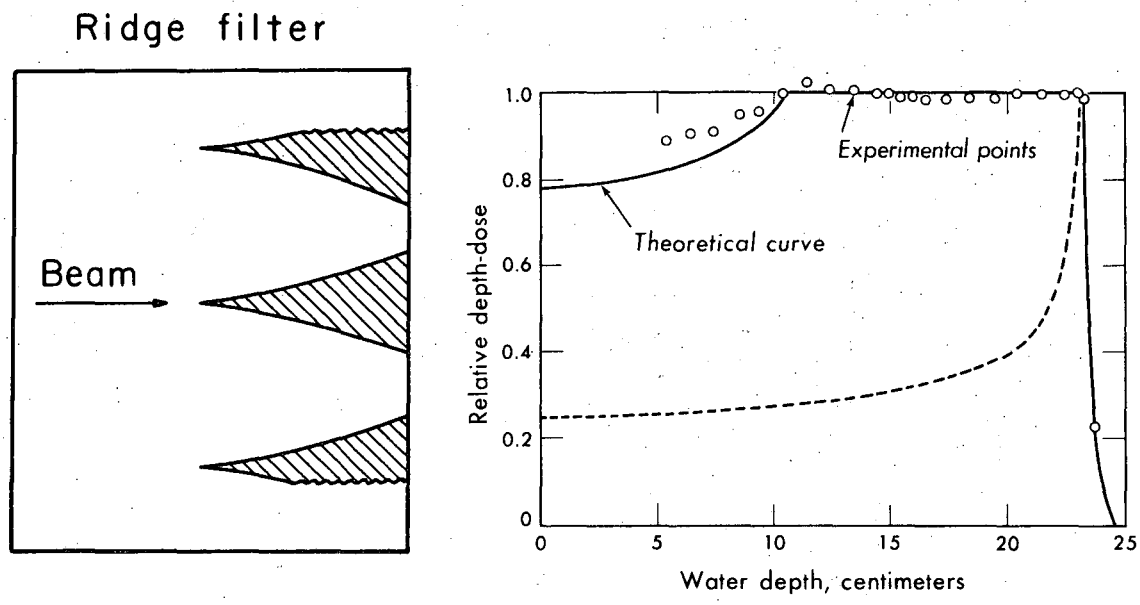

XBL 676-4129

Fig. 24.

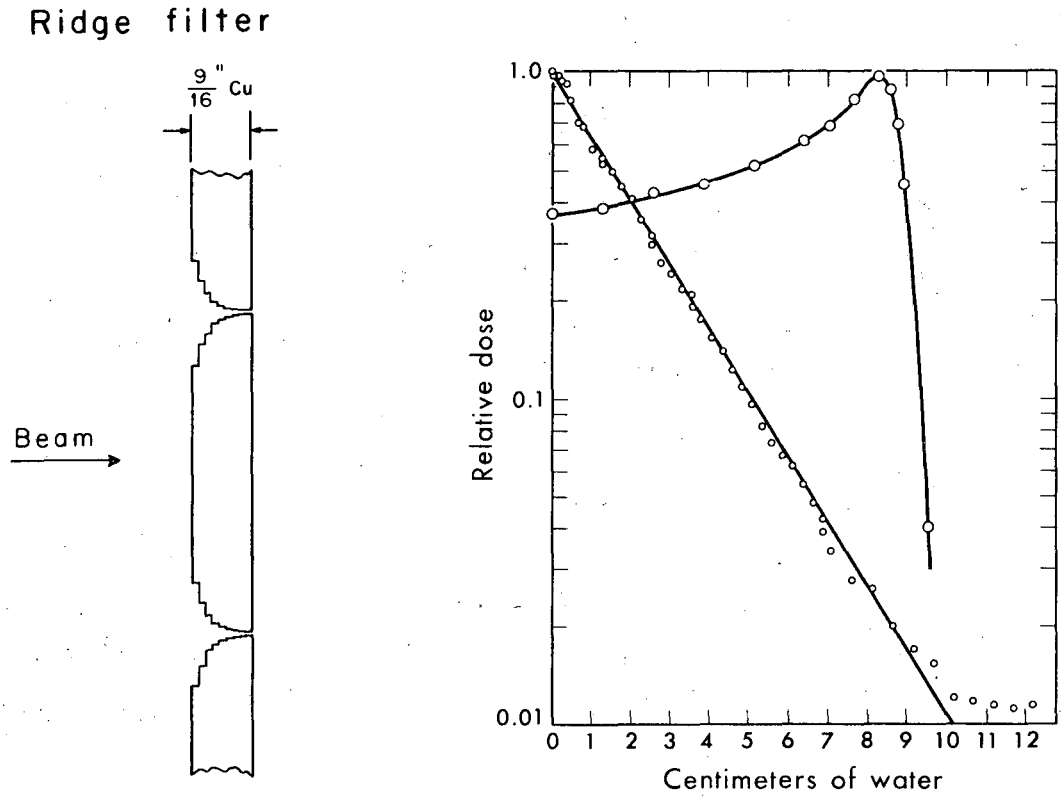

XBL 676-4130

Fig. 25.

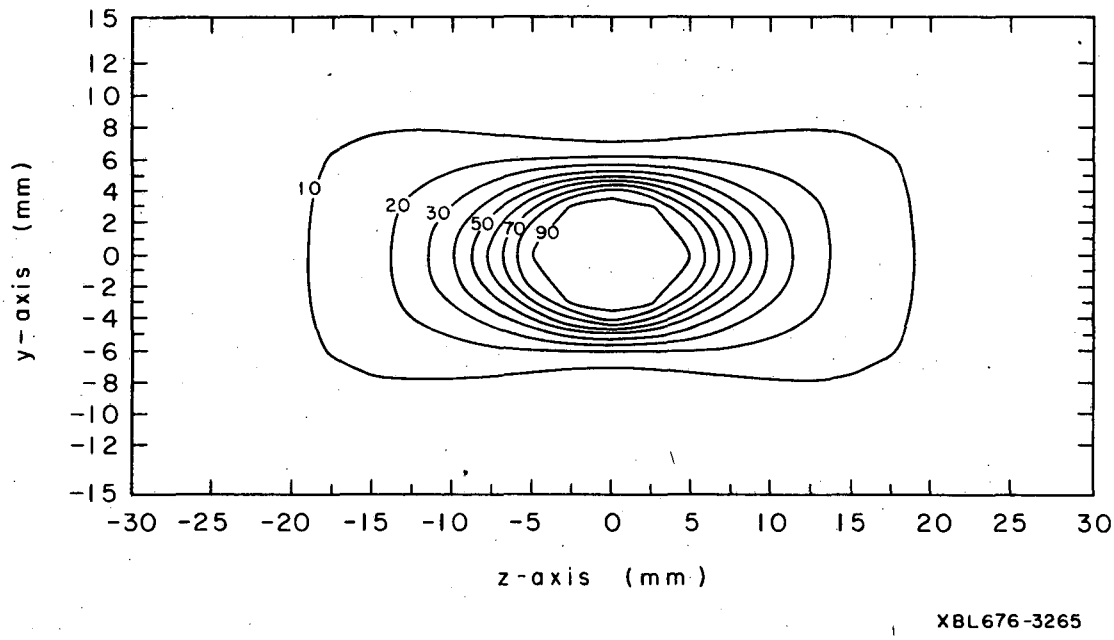
15
12
10
8
6
4
2
0
-2
-4
-6
-8
-10
-12
-15
y-axis (mm)
10
20
30
50
70
90
-30 -25 -20 -15 -10 -5 0 5 10 15 20 25 30
z-axis (mm)
XBL676-3265

Fig. 28.